

T-shaped arrangement of geophones for rapid quantification of asymmetric behaviour of concrete slabs in central FWD tests

Rodrigo Díaz Flores, Mehdi Aminbaghai, Lukas Eberhardsteiner, Ronald Blab, Martin Buchta & Bernhard L. A. Pichler

To cite this article: Rodrigo Díaz Flores, Mehdi Aminbaghai, Lukas Eberhardsteiner, Ronald Blab, Martin Buchta & Bernhard L. A. Pichler (2023) T-shaped arrangement of geophones for rapid quantification of asymmetric behaviour of concrete slabs in central FWD tests, International Journal of Pavement Engineering, 24:1, 2179050, DOI: [10.1080/10298436.2023.2179050](https://doi.org/10.1080/10298436.2023.2179050)

To link to this article: <https://doi.org/10.1080/10298436.2023.2179050>



© 2023 The Author(s). Published by Informa UK Limited, trading as Taylor & Francis Group



Published online: 10 Mar 2023.



Submit your article to this journal [↗](#)



Article views: 381




View related articles [↗](#)



View Crossmark data [↗](#)

T-shaped arrangement of geophones for rapid quantification of asymmetric behaviour of concrete slabs in central FWD tests

Rodrigo Díaz Flores^a, Mehdi Aminbaghai^a, Lukas Eberhardsteiner^b, Ronald Blab^b, Martin Buchta^c and Bernhard L. A. Pichler ^a

^aTU Wien, Institute for Mechanics of Materials and Structures, Vienna, Austria; ^bTU Wien, Institute for Transportation, Vienna, Austria; ^cNievelt Labor GmbH, Höbersdorf, Austria

ABSTRACT

The assessment of asymmetric slab behaviour is out of reach in *standard* Falling Weight Deflectometer (FWD) tests, because deflections are measured along the driving direction only. Herein, a new T-shaped arrangement of the geophones is proposed. It allows for rapid quantification of asymmetric slab behaviour in central FWD testing of concrete slabs. One geophone is positioned at the centre of impact (= centre of the slab), six along the driving direction, one right and one left of the centre. The 'Lateral Asymmetry Index (LASIX)' is introduced as a corresponding dimensionless deflection basin parameter. Its value increases with increasing asymmetric behaviour of the slab. The main research challenge tackled herein is to optimise the radial distance of the lateral geophones from the centre of the slab, such as to maximise the expressiveness of LASIX for the quantification of asymmetric slab behaviour. In this context, FWD tests with measurement of deflections in eight different directions are carried out, and the 'effective asymmetry index (A_{28})' is introduced as another new dimensionless deflection basin parameter. It summarises the asymmetric behaviour based on deflection differences quantified for all 28 pairs of directions which can be combined out of the eight available measurement directions. The optimal radial distance of the lateral geophones from the centre of the slab is found as 1.20 m. Corresponding values of LASIX larger than 8% refer to coefficients of directional variation of the AREA7 parameter larger than 5%. This indicates directional degradation of the pavement structure resulting from eccentric traffic loads. T-shaped FWD testing requires in situ efforts equivalent to those of standard testing, while allowing for a rapid and reliable quantification of asymmetric behaviour. It allows for the assessment of whether the standard evaluation of *uniform* moduli of subgrade reaction is realistic or questionable.

ARTICLE HISTORY

Received 21 October 2022

Accepted 3 February 2023

KEYWORDS

Concrete slabs; falling weight deflectometer; FWD; multi-directional testing; T-shaped testing; deflection basin parameters; asymmetric slab behaviour

1. Introduction

Falling Weight Deflectometry (FWD) is frequently used for non-destructive characterisation of concrete slabs. An FWD test consists of dropping a falling weight (= standardised mass) from a defined height onto a load plate placed on top of the pavement's surface. During the impact, geophones (= displacement sensors) measure the deflection history of several points at the surface of the pavement.

During standard FWD tests, surface deflections are measured along the driving direction, see [Figure 1\(a\)](#). Several modifications to the standard FWD testing have been developed, e.g. the Light Weight Deflectometer which is a portable device used at places inaccessible to FWD-vehicles ([Fleming et al., 2007](#), [Nazzal et al., 2007](#)), the Rolling Weight Deflectometer which performs measurements by means of a loaded wheel running over the pavement of interest ([Bay et al., 1995](#), [Briggs et al., 2000](#)), and the Fast Falling Weight Deflectometer which allows for carrying out a large number of tests in a short period of time ([Pratelli et al., 2018](#), [Coni et al., 2021](#)). All these approaches have in common that deflections are measured along the driving direction. This renders the assessment of asymmetric slab behaviour impossible and provides the motivation for the present paper.

Asymmetric slab behaviour during central FWD tests refers to different deflections recorded at *the same* radial distance from the centre of the slab, but along *different* directions, see [Figure 1\(c\)](#) and ([Díaz Flores et al., 2021](#)). With increasing magnitude of these differences, deflections measured along the driving direction are decreasingly representative of the behaviour of the slab in other directions. This is problematic, because point-symmetric deflection basins are usually assumed when it comes to back-calculation of subgrade stiffness from deflections measured along the driving direction during central FWD tests. Herein, a new T-shaped arrangement of the geophones is proposed for rapid quantification of asymmetric slab behaviour in central FWD testing of concrete slabs.

One geophone is positioned at the centre of impact (= centre of the slab), six along the driving direction (*N*-direction), one right (*E*-direction) and one left (*W*-direction) of the centre, see [Figure 1\(b\)](#), where *N*, *E*, and *W* refer to a local cardinal directional system. As for the quantification of asymmetric structural behaviour, we here introduce a dimensionless deflection basin parameter referred to as 'Lateral Asymmetry Index':

$$\text{LASIX} = \frac{|w_E(r=c) - w_W(r=c)|}{w_N(r=c)}, \quad (1)$$

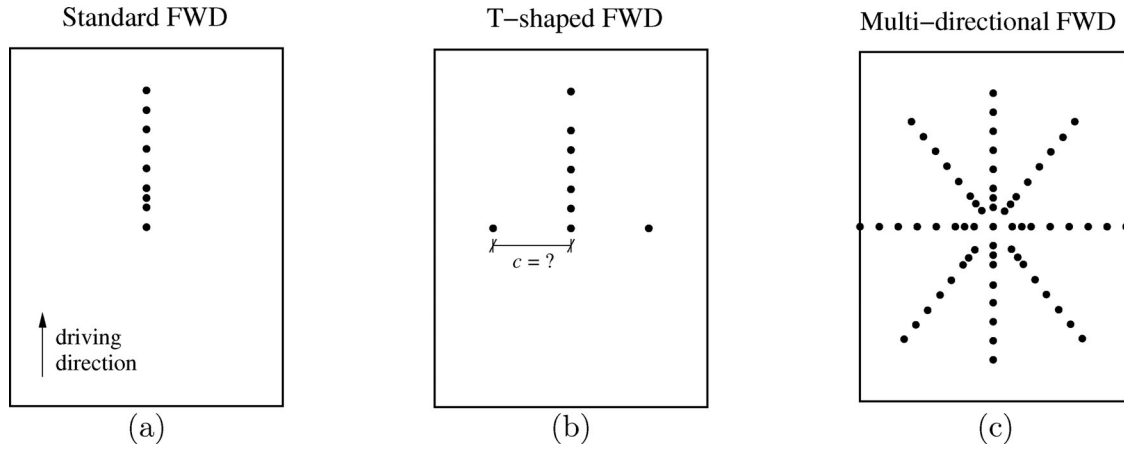


Figure 1. Positions of geophones (see the \bullet symbols) during central FWD testing on rigid pavements: top view onto the (a) standard approach with geophones aligned with the driving direction, (b) proposed T-shaped arrangement, where the lateral distance c is to be optimised, and (c) multi-directional testing according to Díaz Flores *et al.* (2021), providing input data for the aforementioned optimisation.

where $w_E(r=c)$, $w_W(r=c)$, and $w_N(r=c)$ refer to the deflections at the same radial distance $r=c$ from the centre of the slab, but in the E -direction (right), W -direction (left), and N -direction (driving direction), respectively, and $|w_E(r=c) - w_W(r=c)|$ denotes the absolute value of the difference of the deflections measured in the E -direction and the W -direction, at the radial distance $r=c$ from the centre of the slab, see Figure 1(b).

The main research challenge tackled herein is to optimise the radial distance c in Equation (1) such as to maximise the informative content of LASIX regarding the quantification of asymmetric slab behaviour. This optimisation requires the evaluation of LASIX for different values of c and, therefore, the measurement of deflections during central FWD testing on several concrete slabs (i) not only in driving direction, but also right and left of the centre of the slab, and (ii) at several radial distances. The optimal value of c will be determined such that corresponding values of LASIX correlate in the best possible fashion with another newly introduced dimensionless deflection basin parameter: the effective asymmetry index \mathcal{A}_{28} . The latter summarises the asymmetric behaviour of every tested slab in a detailed fashion because it contains information on differences of deflections measured (i) not only in driving direction, right, and left of the centre of the slab, but in *eight* different directions, and (ii) at several radial distances, see Figure 1(c).

The present paper is organised as follows. Section 2 refers to the optimisation of the T-shaped arrangement of geophones based on experimental data from central FWD testing of 10 concrete slabs, with multi-directional measurements of deflections. For all 10 tested slabs, these data provide the basis for quantification (i) of the effective asymmetry index \mathcal{A}_{28} , and (ii) of the lateral asymmetry index LASIX for six different values of c . The optimal distance c will be identified such that associated values of LASIX exhibit the best possible correlation with \mathcal{A}_{28} . Section 3 contains a discussion regarding the sources of asymmetric slab behaviour and their associated implications for the back-calculation of pavement properties from deflections measured during FWD testing. Section 4 contains the conclusions drawn from the results obtained from the presented study.

2. Optimisation of a T-shaped arrangement of geophones for rapid quantification of the asymmetric behaviour of concrete slabs in central FWD tests

2.1. Detailed asymmetry characterisation of 10 concrete slabs subjected to central FWD testing

The development of an optimised T-shaped arrangement of geophones for central FWD testing on concrete slabs requires comprehensive insight into the asymmetries of several slabs. This provides the motivation to perform multi-directional FWD tests (Díaz Flores *et al.*, 2021) at the centres of 10 concrete slabs located on the Austrian highways ‘A1’ and ‘A2’. The tests were performed early in the morning of days during which no significant temperature variations were expected. This excluded problems resulting from slab curling due to temperature gradients (Ioannides and Khazanovich, 1998, Khazanovich *et al.*, 2001).

Five tested slabs are part of the highway ‘A1’. Three of them had been in service for 22 years (‘old slabs’), the other two had been recently installed (‘new slabs’). All slabs have a thickness of 0.22 m and a length of 5.50 m. The widths of the slabs located on the acceleration lane, the first lane, and the emergency lane, are equal to 4.20 m, 3.80 m, and 3.20 m, respectively, see Table 1. The maximum forces imposed during central multi-directional FWD testing range from 201 kN to 203 kN.

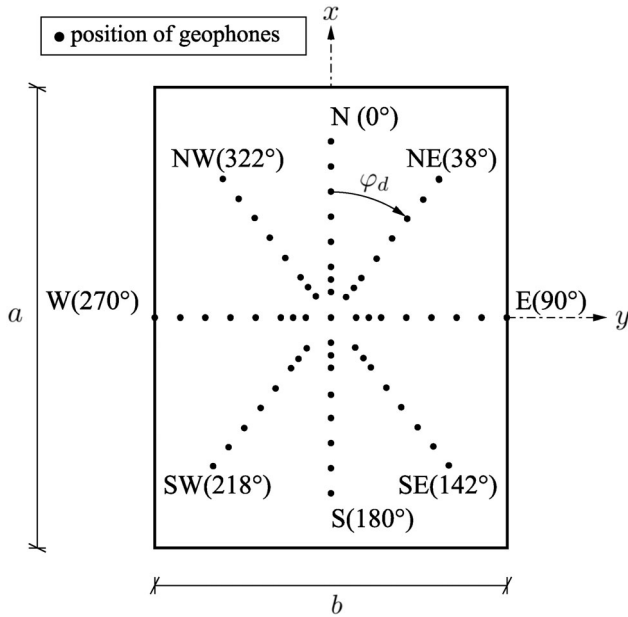
Another five tested slabs are part of the highway ‘A2’. Three of them had been in service for 33 years (‘old slabs’), the other two had been recently installed (‘new slabs’). All slabs have a thickness of 0.22 m. Their length ranges from 4.50 to 5.60 m, and their width from 3.10 to 4.00 m, see Table 1. The maximum forces imposed during central multi-directional FWD testing range from 189 kN to 193 kN.

During multi-directional FWD testing, deflections are measured along eight specific radial directions, starting with the driving direction and proceeding clockwise as described in (Díaz Flores *et al.* 2021), Figure 2, and Table 2, where N, E, S, and W refer to a local cardinal directional system with N pointing in the driving direction. Three tests are carried

Table 1. Properties of the 10 slabs characterised by means of multi-directional FWD testing.

Slab #	Condition	Lane	Length [m]	Width [m]	Thickness [m]	Force [kN]
A1-33354	Old	Acceleration	5.50	4.20	0.22	201
A1-33360	New	Acceleration	5.50	4.20	0.22	201
A1-33868	Old	First	5.50	3.80	0.22	201
A1-33873	New	First	5.50	3.80	0.22	202
A1-33874	Old	Emergency	5.50	3.20	0.22	203
A2-47543	Old	**	4.50	4.00	0.22	193
A2-50000	Old	First	4.50	3.75	0.22	190
A2-51995	New	Emergency	5.60	3.10	0.22	191
A2-54003	Old	First	5.60	3.80	0.22	189
A2-54440	New	First	5.60	3.50	0.22	190

** Transition from acceleration to emergency lane

**Figure 2.** Arrangement of geophones during multi-directional FWD testing according to (Díaz Flores *et al.* 2021), and local cardinal directional system, with N referring to the driving direction.**Table 2.** Polar angles φ_d of the eight different measurement directions.

	Test Direction							
	N	NE	E	SE	S	SW	W	NW
	$d=1$	$d=2$	$d=3$	$d=4$	$d=5$	$d=6$	$d=7$	$d=8$
polar angle	0°	38°	90°	142°	180°	218°	270°	322°

out immediately one after the other in every testing direction, in order to be able to assess test repeatability. After three such tests in all eight measurement directions, another final set of three tests is performed in the N direction, again for the sake of being able to assess test repeatability. Thus, the first and the ninth set of three tests correspond to the N direction.

Table 3. Radial distances of the geophones from the centre of impact (= centre of the slab), $r_{d,g}$ [m], as functions of the measurement direction: $d=1$ (N), $d=2$ (NE), $d=3$ (E), $d=4$ (SE), $d=5$ (S), $d=6$ (SW), $d=7$ (W), $d=8$ (NW).

Test Directions	Geophone								
	$g=1$	$g=2$	$g=3$	$g=4$	$g=5$	$g=6$	$g=7$	$g=8$	$g=9$
$d \in [1, 2, 3, 5, 7, 8]$	0.00	0.30	0.45	0.60	0.90	1.20	1.50	1.80	2.10
$d \in [4, 6]$	0.00	0.45	0.60	0.75	1.05	1.35	1.65	1.95	2.25

During every single FWD test, nine geophones measure deflections of the surface of the slab. The first geophone ($g=1$) is located at the centre of the slab, the other eight ($g=2$ to $g=9$) are fixed to a bar which ensures that the distances between them are constant. Structural constraints of the FWD-device make it necessary to move the bar 15 cm further away from the centre when measuring along the SE and SW directions, as compared to all the other directions, see Table 3.

In case that the outermost geophone(s) are located on the neighbouring slab or on the adjacent soil, their measurements are excluded. The number of excluded geophones are sometimes different in the E and W directions, see Table 4, because of small eccentricities of the FWD-device from the centre of the slab, which amounted to a few single centimetres.

All deflection maxima recorded by the geophones on the 10 tested slabs are listed in Tables A1 to A10. The deflection maxima measured on the slabs A2-54003 and A2-54440 are exemplarily illustrated in Figure 3.

Test repeatability is satisfactory. The three to six (six tests were performed in driving direction, three tests in all other directions) tests performed in every direction delivered very similar deflection maxima in all radial distances, see e.g. the red zoom windows in Figure 3(a) and (c). In all 27 tests performed per slab, the deflection maxima measured at the centre of impact are very similar, see the first columns of measured data in Tables A1 to A10. The first three tests and the last three tests, referring to the driving direction, delivered very similar results see e.g. the red zoom windows in Figure 3(a) and (c) as well as data in Tables A1 to A10. This underlines that the support conditions of the 10 characterised slabs were stable during the approximately 45 minutes needed to perform a complete set of multi-directional FWD tests.

2.2. Quantification of the asymmetry of the structural behaviour by means of the new deflection basin parameter A_{28}

The deviation of the structural behaviour of the tested slabs from point symmetry with respect to the centre of impact (=

Table 4. Geophones which were excluded since they were located outside the tested slab.

Tested Slab	Direction	Excluded geophones
A1-33354	W	$g = 9$
A1-33360	W	$g = 9$
A1-33868	W	$g = 9$
	E	$g \in \{8, 9\}$
A1-33873	W	$g = 9$
	E	$g \in \{8, 9\}$
A1-33874	W	$g = 9$
	E	$g \in \{8, 9\}$
A2-47543	W	$g = 9$
	E	$g = 9$
A2-50000	W	$g = 9$
	E	$g \in \{8, 9\}$
A2-51995	W	$g \in \{7, 8, 9\}$
	E	$g \in \{8, 9\}$
A2-54003	W	$g \in \{8, 9\}$
	E	$g = 9$
A2-54440	W	$g \in \{8, 9\}$
	E	$g = 9$

centre of the slab) is quantified by means of the ‘effective asymmetry index’ which is a new deflection basin parameter introduced as

$$\mathcal{A}_{28} = \sqrt{\frac{1}{28} \sum_{j=1}^{28} (A_{d,\delta})^2}, \quad (2)$$

where the relation between the summation index j and asymmetry indicators $A_{d,\delta}$ is clarified in Table 5. The values of $A_{d,\delta}$ quantify differences of deflections measured in two *different* directions d and δ , as introduced in (Díaz Flores *et al.*, 2021), as

$$A_{d,\delta} = \sqrt{\frac{1}{\ell} \int_0^\ell \left[\frac{w_d(r)}{w_d(r=0)} - \frac{w_\delta(r)}{w_\delta(r=0)} \right]^2 dr}, \quad (3)$$

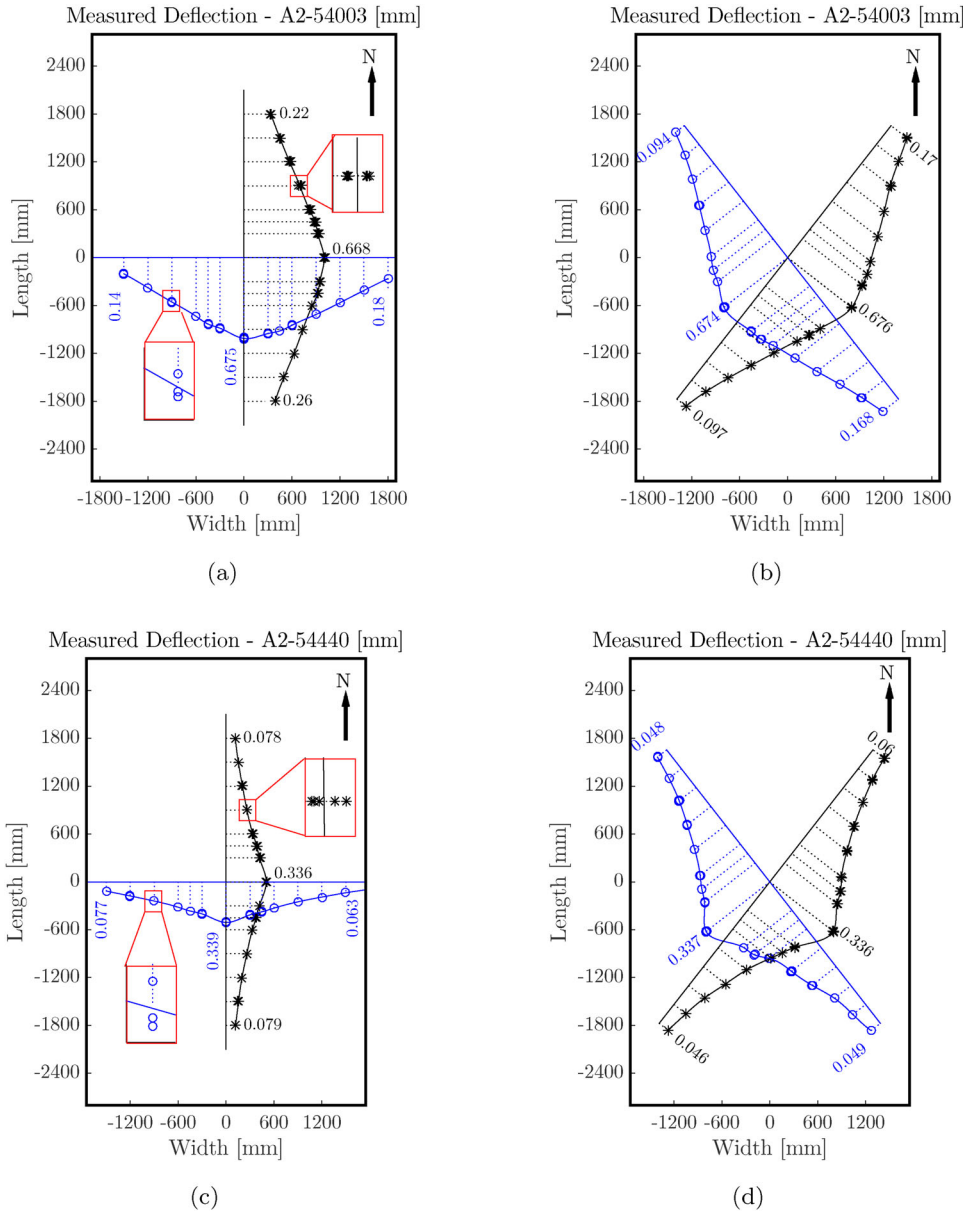


Figure 3. Results from multi-directional FWD testing on the old slab A2-54003, see (a) and (b), as well as on the new slab A2-54440, see (c) and (d): the points refer to the deflection maxima listed in Tables A9 and A10, respectively, measured by the geophones along the N, S, E and W directions, see (a) and (c), as well as along the SE, SW, and NW directions, see (b) and (d); the solid lines refer to splines interpolating between the average of the three (to six) deflections measured at each location.

Table 5. Asymmetry indicators, $A_{d,\delta}$ according to Equation (3), quantifying the deviation of the measured structural behaviour from point symmetry with respect to the centre of impact (= centre of the slab); evaluated for the 10 tested slabs.

Slab # Condition		A1-33354 Old	A1-33360 New	A1-33868 Old	A1-33873 New	A1-33874 Old	A2-47543 Old	A2-50000 Old	A2-51995 New	A2-54003 Old	A2-54440 New
$A_{N,NE}$	$j=1$	2.63%	5.25%	3.50%	1.55%	1.40%	3.25%	0.78%	1.13%	1.24%	0.49%
$A_{N,E}$	$j=2$	4.18%	6.91%	8.85%	4.20%	3.73%	8.23%	1.69%	1.28%	2.97%	2.93%
$A_{N,SE}$	$j=3$	7.48%	4.14%	1.37%	2.55%	3.72%	1.55%	8.90%	1.22%	5.99%	1.60%
$A_{N,S}$	$j=4$	4.94%	3.98%	2.30%	1.65%	2.16%	2.41%	5.98%	0.98%	3.96%	0.68%
$A_{N,SW}$	$j=5$	1.71%	5.25%	3.79%	2.11%	2.70%	5.33%	3.98%	3.04%	3.85%	1.56%
$A_{N,W}$	$j=6$	9.68%	6.26%	2.26%	2.40%	3.59%	2.63%	6.10%	5.42%	14.21%	4.95%
$A_{N,NW}$	$j=7$	6.76%	3.92%	2.87%	3.10%	3.17%	4.24%	4.87%	4.74%	9.68%	3.49%
$A_{NE,E}$	$j=8$	1.75%	1.87%	5.44%	2.11%	2.64%	5.82%	1.67%	1.99%	3.18%	2.33%
$A_{NE,SE}$	$j=9$	4.98%	3.09%	3.00%	1.96%	3.53%	2.29%	8.44%	1.20%	4.94%	1.84%
$A_{NE,S}$	$j=10$	2.52%	2.54%	6.07%	2.52%	3.01%	4.98%	5.44%	1.62%	2.98%	0.98%
$A_{NE,SW}$	$j=11$	3.01%	4.44%	7.17%	3.03%	3.99%	7.83%	3.63%	4.01%	4.88%	1.43%
$A_{NE,W}$	$j=12$	9.75%	3.68%	3.07%	1.46%	5.48%	5.10%	6.45%	6.74%	14.70%	3.77%
$A_{NE,NW}$	$j=13$	7.47%	2.55%	2.29%	1.24%	4.14%	2.88%	5.29%	6.08%	10.15%	3.11%
$A_{E,SE}$	$j=14$	4.97%	3.02%	8.27%	3.66%	3.74%	6.14%	5.63%	2.37%	7.68%	4.69%
$A_{E,S}$	$j=15$	2.62%	3.98%	10.97%	4.02%	4.46%	8.25%	3.37%	1.31%	6.14%	2.70%
$A_{E,SW}$	$j=16$	4.54%	4.66%	12.63%	4.49%	4.69%	12.49%	3.14%	2.61%	2.93%	2.32%
$A_{E,W}$	$j=17$	12.00%	3.49%	7.56%	2.98%	7.75%	8.60%	5.94%	5.83%	13.95%	1.78%
$A_{E,NW}$	$j=18$	9.03%	3.65%	7.72%	1.14%	5.74%	8.01%	6.37%	5.02%	7.87%	0.89%
$A_{SE,S}$	$j=19$	2.72%	1.14%	3.48%	2.78%	2.94%	2.90%	3.95%	1.40%	2.27%	1.71%
$A_{SE,SW}$	$j=20$	7.34%	2.43%	4.31%	2.62%	4.35%	5.79%	5.96%	3.57%	9.67%	2.03%
$A_{SE,W}$	$j=21$	14.88%	1.99%	1.77%	1.45%	6.91%	3.79%	14.32%	6.41%	19.11%	5.28%
$A_{SE,NW}$	$j=22$	12.19%	1.24%	1.38%	1.63%	6.63%	1.45%	13.37%	5.98%	15.03%	4.31%
$A_{S,SW}$	$j=23$	4.88%	2.51%	1.61%	1.85%	1.90%	2.99%	2.75%	2.63%	7.76%	1.54%
$A_{S,W}$	$j=24$	13.53%	2.95%	4.19%	2.23%	4.00%	2.86%	11.37%	4.89%	18.06%	4.39%
$A_{S,NW}$	$j=25$	9.58%	0.54%	3.96%	3.19%	4.28%	2.74%	10.69%	4.83%	13.00%	3.63%
$A_{SW,W}$	$j=26$	7.58%	2.48%	5.03%	2.48%	3.24%	4.49%	9.08%	3.42%	10.67%	3.52%
$A_{SW,NW}$	$j=27$	5.05%	2.79%	5.03%	3.57%	3.42%	5.58%	8.60%	3.15%	5.44%	2.84%
$A_{W,NW}$	$j=28$	2.40%	2.73%	1.49%	1.60%	1.86%	3.85%	1.72%	1.41%	5.94%	1.47%

where both indexes d and δ run over the eight measurement directions: N, NE, E, SE, S, SW, W, and NW. Also in Equation (3), r denotes the radial coordinate, while $w_d(r)$ and $w_\delta(r)$ stand for splines referring to the measurement directions d and δ , respectively. These splines (see e.g. the blue and black solid lines in Figure 3) interpolate between the average of the three (to six) deflection maxima measured at each point. Finally, ℓ denotes the radial length of integration. Here, ℓ is equal to 2.10 m, except when comparing directions along which geophones were excluded, see Table 4. In these cases, ℓ is equal to the distance from the centre of the slab to the last geophone that was included.

For every one of the 10 tested slabs, asymmetry indicators are evaluated according to Equation (3) for all 28 combinations of two different directions out of the available eight measurement directions. The $10 \times 28 = 280$ asymmetry indicators are listed in Table 5.

A_{28} according to Equation (2) refers to multi-directional FWD testing in eight different directions. The subscript ‘28’

to all 28 combinations of two different directions out of the eight available measurement directions. The effective asymmetry index A_{28} of every slab is obtained from inserting its 28 asymmetry indicators from Table 5 into Equation (2), see Table 6 for the results. The 10 obtained effective asymmetry indices allow for the correct classification of the tested slabs into ‘old slabs’ and ‘new slabs’, because A_{28} of all old/new slabs is larger/smaller than 4%. This corroborates the expressiveness of A_{28} regarding the assessment of asymmetric structural behaviour.

2.3. Quantification of asymmetric structural behaviour based on T-shaped testing and the deflection basin parameter LASIX

A T-shaped arrangement of geophones is proposed with the aim to combine the advantages of standard and multi-directional FWD testing: (i) rapid in situ characterisation and (ii) expressiveness regarding the assessment of asymmetric structural behaviour. Surface deflections are measured by means of nine geophones: one at the centre of impact (= centre of the slab), six along the driving direction, one left and one right of the centre of impact, see Figure 1(b).

The corresponding assessment of asymmetric structural behaviour is based on the deflection basin parameter LASIX, introduced in Equation (1). The remaining open research question refers to optimising the radial distance c of the geophones from the centre of the slab, in order to maximise the informative content of LASIX for the quantification of asymmetric slab behaviour. This optimisation requires an evaluation of LASIX for different values of c , which is possible, because multi-directional testing delivers geophone

Table 6. Values of the effective asymmetry index, A_{28} according to Equation (2), calculated for the 10 tested slabs; integrating the 28 asymmetry indicators of each slab (see Table 5) into one single value.

Slab #	Condition	A_{28}
A1-33354	Old	7.68%
A1-33360	New	3.81%
A1-33868	Old	5.54%
A1-33873	New	2.73%
A1-33874	Old	4.29%
A2-47543	Old	5.52%
A2-50000	Old	7.35%
A2-51995	New	3.87%
A2-54003	Old	9.67%
A2-54440	New	2.94%

Table 7. Lateral Asymmetry Index, LASIX according to Equation (1), evaluated for different radial distances c of the geophones in E, W, and N directions.

Slab #	Condition	$c = 0.30$ m	$c = 0.45$ m	$c = 0.60$ m	$c = 0.90$ m	$c = 1.20$ m	$c = 1.50$ m
A1-33354	Old	12.47%	14.07%	16.11%	18.54%	16.93%	12.66%
A1-33360	New	4.72%	5.23%	4.51%	2.83%	0.31%	1.79%
A1-33868	Old	3.73%	7.27%	9.21%	10.84%	8.98%	5.95%
A1-33873	New	2.89%	2.72%	2.16%	0.80%	0.29%	2.87%
A1-33874	Old	0.74%	0.33%	1.09%	5.04%	9.28%	12.34%
A2-47543	Old	0.22%	2.70%	5.53%	9.09%	10.43%	7.79%
A2-50000	Old	1.55%	4.87%	6.58%	8.35%	9.56%	10.15%
A2-51995	New	3.12%	6.23%	5.98%	6.74%	7.10%	
A2-54003	Old	6.74%	8.60%	11.21%	15.54%	18.62%	20.64%
A2-54440	New	2.44%	1.92%	2.37%	2.02%	2.76%	4.29%

measurements at so many positions, that focusing on subsets of the available geophone positions allows for simulating T-shaped arrangements of the geophones with several different values of c . LASIX is evaluated according to Equation (1) for six different values of c (0.30 m, 0.45 m, 0.60 m, 0.90 m, 1.20 m, and 1.50 m) and for all 10 slabs, see Table 7.

2.4. Optimal distance c of the lateral geophones from the centre of the slab

The optimal radial distance c of the geophones from the centre of impact refers to the largest possible expressiveness of LASIX for the assessment of asymmetric structural behaviour. The related optimisation problem is solved as follows. For all six different values of c (0.30 m, 0.45 m, 0.60 m, 0.90 m, 1.20 m, and 1.50 m) the following steps are performed:

- (1) Ten values of LASIX, referring to T-shaped testing with one specific value of c , see the respective columns in Table 7, are correlated with the 10 corresponding values of \mathcal{A}_{28} derived from multi-directional testing, see Table 6.
- (2) The best linear regression function is fitted to the pairs of values of LASIX and \mathcal{A}_{28} , and the corresponding quadratic correlation coefficient is determined, see Table 8.

The best correlation between LASIX, related to T-shaped FWD testing, and \mathcal{A}_{28} , related to multi-directional FWD testing, is obtained for deflections measured at a distance $c = 1.20$ m from the centre of the slab, see Table 8. The corresponding maximum of the quadratic correlation coefficient amounts to $R^2 = 82\%$, see also Figure 4. The values of LASIX referring to $c = 1.20$ m allow for the correct classification of the tested slabs into ‘old slabs’ and ‘new slabs’. As for all new slabs, values of LASIX referring to $c = 1.20$ m are smaller than or equal to 7.10%. As for all old slabs, values of LASIX referring to $c = 1.20$ m are larger than or equal to 8.98%. This underlines the expressiveness of the newly introduced deflection-basin-parameter LASIX regarding the

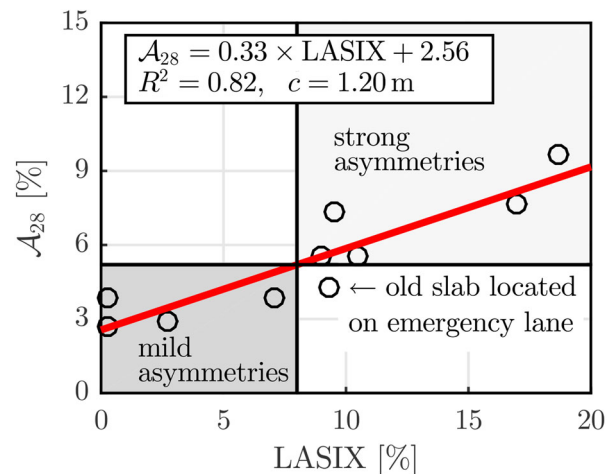
Table 8. Correlation between the values of LASIX in Table 7, referring to different values of the distance c , and values of \mathcal{A}_{28} listed in Table 6.

distance	best linear regression function	R^2
$c = 0.30$ m	$\mathcal{A}_{28} = 0.32 \times \text{LASIX} + 4.12$	25%
$c = 0.45$ m	$\mathcal{A}_{28} = 0.37 \times \text{LASIX} + 3.34$	42%
$c = 0.60$ m	$\mathcal{A}_{28} = 0.39 \times \text{LASIX} + 2.84$	61%
$c = 0.90$ m	$\mathcal{A}_{28} = 0.35 \times \text{LASIX} + 2.57$	78%
$c = 1.20$ m	$\mathcal{A}_{28} = 0.33 \times \text{LASIX} + 2.56$	82%
$c = 1.50$ m	$\mathcal{A}_{28} = 0.35 \times \text{LASIX} + 2.44$	74%

assessment of asymmetric structural behaviour. In Figure 4, the threshold value of LASIX distinguishing old from new slabs was set equal to 8.00%.

The threshold value LASIX = 8% refers, according to the red regression line in Figure 4, to $\mathcal{A}_{28} = 5.2\%$. This threshold value allows for the correct classification into old and new slabs in all but one case: the old slab A1-33874 with LASIX = 10.43% ($> 8\%$) and $\mathcal{A}_{28} = 4.29\%$ ($< 5.2\%$), see Tables 7 and 6. Notably, this slab was part of an emergency lane, see Table 1. Therefore, it was subjected to traffic loading only indirectly, namely, because of load transfer via tie bars connecting the tested slab to its neighbour which was part of the first lane and, therefore, directly exposed to traffic loads. This underlines that values of LASIX $> 8\%$ call for an engineering assessment of the specific exposure of the tested slab to eccentric traffic loads.

The construction of trailers containing a fixed installation of the optimal T-shaped arrangement of geophones appears to be feasible, because the optimal distance between the two lateral geophones, $2 \times c = 2.40$ m, is smaller than the maximum allowed width of vehicles. Such trailers will facilitate in situ data acquisition, because the operators can stay inside their vehicle, as in standard FWD testing, i.e. there is no need for the operators to get out of their vehicle and manipulate the geophones, as required for multi-directional FWD testing.

**Figure 4.** Best correlation between the Lateral Asymmetry Index LASIX according to Equation (1), related to T-shaped FWD testing, and the effective asymmetry index \mathcal{A}_{28} according to Equation (2), related to multi-directional FWD testing: the deflections w_E , w_W , and w_N used to evaluate LASIX were measured at a distance $c = 1.20$ m from the centre of impact; each symbol corresponds to one of the 10 tested slabs; the horizontal and vertical black lines represent the threshold values of \mathcal{A}_{28} and LASIX distinguishing mild from strong asymmetries.

2.5. Arrangement of the geophones remaining aligned with the driving direction

As for the six geophones which remain aligned with the driving direction, it is proposed to arrange them at radial distances amounting to 0.30 m, 0.60 m, 0.90 m, 1.20 m, 1.50 m, and 2.10 m from the centre of the slab. Relative to standard FWD testing, the geophones at radial distances $r = 0.45$ m and $r = 1.80$ m are missing in the case of T-shaped

FWD testing, because they are needed right and left of the centre of the slab.

The associated loss of information regarding deflections measured along the driving direction is assessed as follows. Splines are used for interpolation between the deflections measured along the driving direction during T-shaped testing, see the blue lines and the black circles in Figures 5 and 6. They are evaluated at the positions of the removed

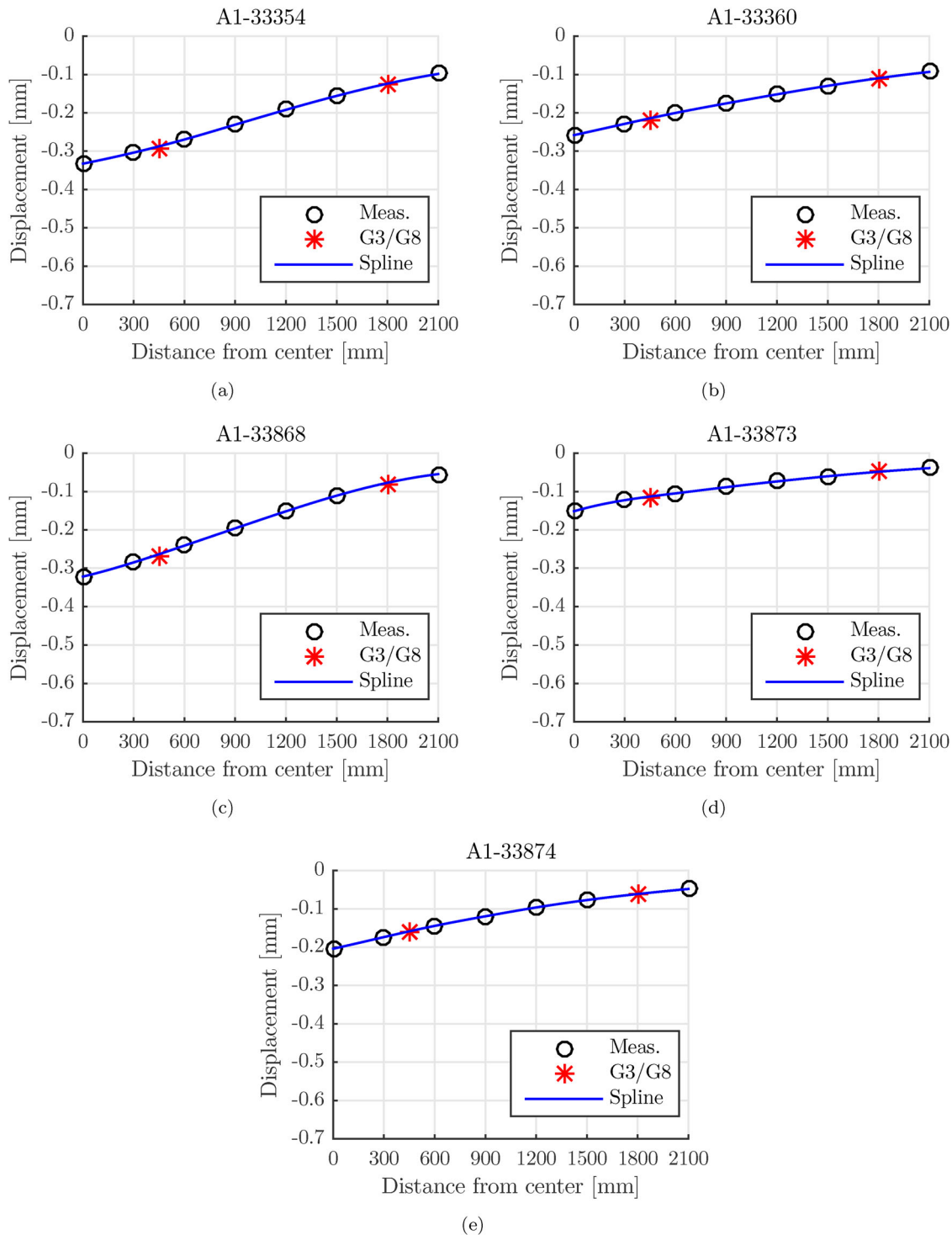


Figure 5. Deflections measured by geophones 3 and 8 (red stars, $r = 450$ mm and $r = 1800$ mm, respectively), and spline (blue line) interpolating between the rest of deflections measured in the driving direction (black circles), for slabs (a) A1-33354, (b) A1-33360, (c) A1-33868, (d) A1-33873, (e) A1-33874.

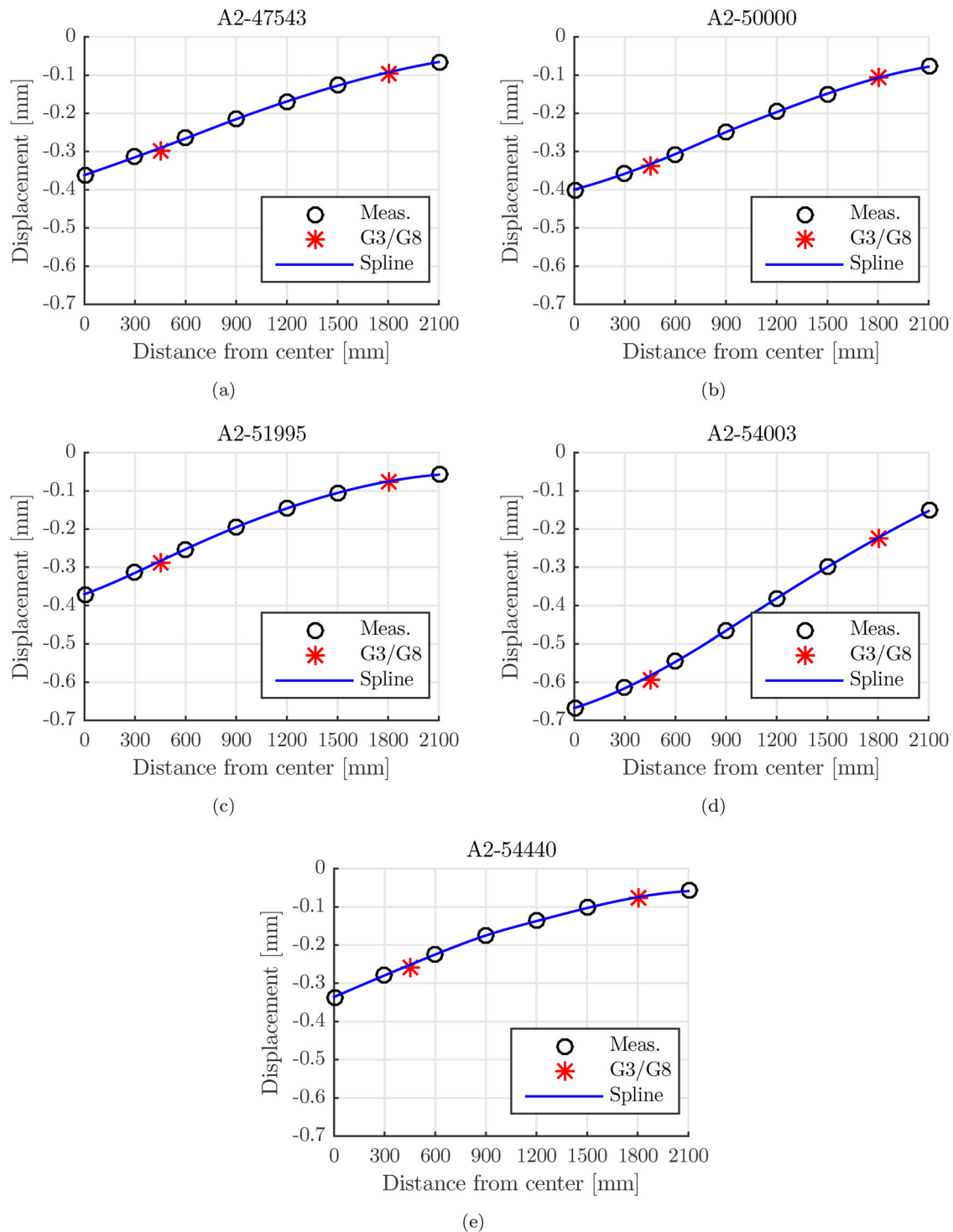


Figure 6. Deflections measured by geophones 3 and 8 (red stars, $r = 450$ mm and $r = 1800$ mm, respectively), and spline (blue line) interpolating between the rest of deflections measured in the driving direction (black circles), for slabs (a) A2-47543, (b) A2-50000, (c) A2-51995, (d) A2-54003, (e) A2-54440.

geophones (i.e. at $r = 0.45$ m and $r = 1.80$ m, respectively). The resulting spline-interpolated values are compared with deflections measured during multi-directional testing at these positions, see the red stars in Figures 5 and 6. The relative error between spline-interpolated (index *int*) and measured (index *m*) values, $|\frac{w_{int}(r) - w_m(r)}{w_m(r)}|$, is smaller than 4% for all 10 tested slabs and at both positions from which geophones were removed, see Table 9. Thus, the loss of information resulting from the re-arrangement of two

geophones from the driving direction to the lateral positions is tolerable for engineering purposes.

3. Discussion

Central FWD tests with the developed T-shaped arrangement of geophones, and their evaluation by means of quantification of LASIX according to Equation (1), was shown to provide a reliable assessment of asymmetric structural behaviour of

Table 9. Values of the mean deflections measured ($w_m(r)$) by the geophones at radial distances of $r = 0.45$ m and $r = 1.80$ m from the centre of the slab, and values of the deflections ($w_{int}(r)$), at the same locations, obtained from the spline interpolating between the measurements of the rest of the geophones along the driving direction, for all 10 slabs, as well as the relative error between them.

Slab #	measured deflection $w_m(r = 0.45 \text{ m})$	spline-interpolated deflection $w_{int}(r = 0.45 \text{ m})$	relative error $\frac{ w_{int} - w_m }{w_m}$	measured deflection $w_m(r = 1.80 \text{ m})$	spline-interpolated deflection $w_{int}(r = 1.80 \text{ m})$	relative error $\frac{ w_{int} - w_m }{w_m}$
A1-33354	0.292 mm	0.287 mm	1.7%	0.127 mm	0.124 mm	2.4%
A1-33360	0.218 mm	0.214 mm	1.8%	0.111 mm	0.110 mm	0.9%
A1-33868	0.269 mm	0.263 mm	2.3%	0.079 mm	0.077 mm	2.5%
A1-33873	0.116 mm	0.113 mm	2.6%	0.047 mm	0.048 mm	2.1%
A1-33874	0.160 mm	0.159 mm	0.6%	0.062 mm	0.061 mm	1.6%
A2-47543	0.297 mm	0.291 mm	2.0%	0.094 mm	0.093 mm	1.1%
A2-50000	0.338 mm	0.333 mm	1.5%	0.108 mm	0.107 mm	0.9%
A2-51995	0.287 mm	0.284 mm	1.1%	0.076 mm	0.075 mm	1.3%
A2-54003	0.593 mm	0.583 mm	1.7%	0.224 mm	0.223 mm	0.5%
A2-54440	0.257 mm	0.252 mm	2.0%	0.078 mm	0.075 mm	3.8%

rigid pavements. The following discussion deals with the question of where do such asymmetries come from, and with implications for the back-calculation of subgrade properties.

3.1. Reasons for asymmetric slab behaviour

Values of the effective asymmetry index \mathcal{A}_{28} of the four new slabs range from 2.73% to 3.87%, see Table 6. The corresponding mean value amounts to 3.33%. Thus, even new slabs exhibit asymmetric structural behaviour when subjected to central FWD testing.

The reason for an asymmetric behaviour in new slabs can be explained by their *finite size* as well as *slab-to-slab interaction* through dowels and tie bars (it is unlikely that a non-uniform distribution of subgrade stiffness is responsible for asymmetric behaviour of new slabs, because methods such as the dynamic compaction control are used during construction to ensure that all subgrade layers of pavement structure have uniform properties). The dense arrangement of dowels (typical spacing: 25 to 30 cm) render slab-to-slab load transfer in driving direction effective. Dowel-connected new slabs thus almost behave as if they were continuous in driving direction. The less dense arrangement of tie bars (typical spacing: 150 cm) renders the load transfer in lateral direction less effective. In addition, many slabs are connected by means of tie bars to a neighbour on one side, while the opposite lateral edge is free. Differences in boundary conditions of the edges of the slabs, together with their rectangular (rather than quadratic) shape, render their behaviour asymmetric already right after construction. The deviations from point symmetry are quantified through \mathcal{A}_{28} .

Values of \mathcal{A}_{28} of the six old slabs range from 4.29% to 9.67%, see Table 6. The corresponding mean value amounts to 6.67%. This underlines that the old slabs showed, on average, twice as much asymmetric structural behaviour than the new slabs. Recurrent loading over many years is responsible for the increase of the asymmetries. Notably, traffic loads are *eccentric* in the standard case that tire tracks are asymmetrically arranged relative to the *N-S*-axis running through the centre of the slabs, see Figure 7. The corresponding asymmetric fatigue loading results in a directional deterioration of the pavement structure. This yields increasing deviations from point-symmetric behaviour in central FWD testing and, therefore, increasing values of \mathcal{A}_{28} . As regards ‘eccentric’ traffic loads, it is noteworthy that it is currently ensured by

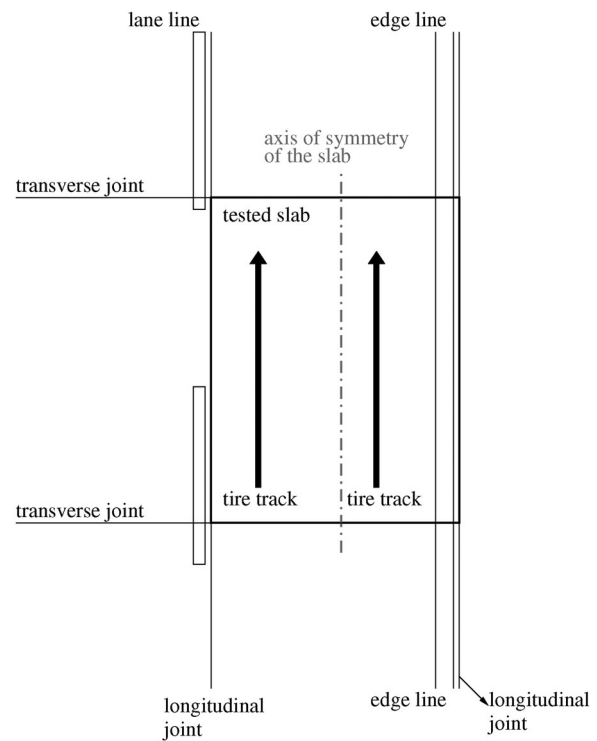


Figure 7. Top view onto a slab subjected to eccentric long-term loading resulting from tire tracks which are asymmetrically arranged relative to the *N-S*-axis running through the centre of the slab.

design that the tire tracks run as far away as possible from the free edges of the slab (those facing the shoulder). As a consequence, edge stresses are minimised and the fatigue life of the pavement is extended. In addition, some design methods include the option of installing a tied shoulder beyond the traffic lanes, with the aim of either improving service life or reducing the required slab thickness, see e.g. (Packard, 1984, Packard and Tayabji, 1985).

Imperfect positioning of the falling weight also contributes to asymmetric structural behaviour. An eccentric positioning in driving direction has a smaller influence than the same eccentricity in lateral direction, because of the following two reasons:

- (1) Eccentricities of the falling weight are to be related to the size of the tested slab. The lateral width of slabs is smaller than their length. Thus, the same eccentricity in both

directions leads to a larger effective imperfection in lateral direction. Similarly, if different slabs are tested with the same unintentional lateral eccentricity, its influence will be the larger the smaller the lateral width of the tested slab.

- (2) If dowel-connected slabs almost behave as if they were continuous in driving direction, eccentricities in driving direction will not result in significant asymmetries. Lateral eccentricities, in turn, must be expected to particularly increase asymmetries of slabs which are connected by means of tie bars to a neighbour on one side, while the opposite lateral edge is free.

All described FWD tests on new plates were carried out with small eccentricities of the FWD-device from the centre of the slab, amounting to a few single centimetres. The resulting asymmetries were small enough that \mathcal{A}_{28} allowed for the correct classification into new and old slabs. This underlines that asymmetries arising from unintentional eccentric FWD testing are implicitly considered in the threshold value of $\mathcal{A}_{28} = 5.2\%$, distinguishing newly built from directionally degraded pavement structures.

3.2. Back-calculation of subgrade properties based on deflections known from FWD testing

Surface deflections measured during FWD testing are functions of the loading exerted by the falling weight and of the properties of the pavement structure. Thus, it is conceptually possible to back-calculate properties of the pavement structure from known surface loading and deflections. To the best of the authors' knowledge all currently available back-calculation approaches assume a uniform distribution of subgrade stiffness and, therefore, a symmetric behaviour of pavement structures. This assumption is challenged by the asymmetric structural behaviour found by means of multi-directional FWD testing of old slabs. In the following, 'dense liquid' models as well as the corresponding AREA and Best Fit methods will be briefly summarised. This provides the basis for subsequent correlation of LASIX with the directional variation of the deflection basin parameter AREA7, see Section 3.3.

The 'dense-liquid' model (AASHTO, 2008) idealises rigid pavements as infinite thin elastic plates on a uniform Winkler foundation (Winkler, 1867). There are two different back-calculation approaches: the AREA method and the Best Fit method. Both of them are based on closed-form solutions, which can be traced back to (Westergaard, 1926). Back-calculation concerns identification of the radius of relative stiffness, l_k , from surface deflections measured during FWD testing. l_k is equal to $(D/k)^{0.25}$, where D denotes the bending stiffness of the plate and k the modulus of subgrade reaction of the Winkler foundation. Formulae for the final transition from l_k to the modulus of subgrade reaction were proposed, see e.g. (Darter *et al.* 1995, Hall *et al.*, 1997). They have become part of the mechanistic-empirical design and evaluation of rigid pavements (AASHTO, 2008, Smith *et al.*, 2017).

The AREA method is based on the AREA parameter. It was originally introduced as the area (hence the name) under the graph showing surface deflections of the pavement structure over the radial distance from the falling weight (Hoffman

and Thompson, 1980). In order to account for different amplitudes of the falling weight, which yield qualitatively similar but quantitatively different surface deflections, the latter were normalised with respect to their maximum value, w_0 , measured at the position of the falling weight (Hoffman and Thompson, 1980). Therefore, the *normalised* version of the AREA parameter has the physical dimension of a length rather than an area. As for a configuration of four geophones with a uniform spacing equal to Δr , it reads as

$$\begin{aligned} \text{AREA} &= \frac{1}{w_0} \int_0^{3\Delta r} w(r) dr \\ &\approx \frac{\Delta r}{2 w_0} [w_0 + 2 w_1 + 2 w_2 + w_3], \end{aligned} \quad (4)$$

where w_γ refers to the deflection measured by the geophone at the radial distance of $r = \gamma \Delta r$. The last expression in Equation (4) refers to numerical integration using the trapezoidal rule. Inspired by a dimensionless representation of Westergaard's solution by Losberg (1960), Ioannides (1990) used dimensional analysis for the derivation of a relation between the AREA parameter according to Equation (4) and the radius of relative stiffness, see Figure 3 in (Ioannides, 1990). Other sensor configurations were studied e.g. by Hall and Mohseni (1991). The method that is based on four measured deflections is referred to as 'AREA4', the one based on seven measured deflections as 'AREA7'. Both of them are used for rigid pavements (Khazanovich *et al.*, 2001).

The Best Fit method is also based on a dimensionless representation of Westergaard's solution by Losberg (1960). A closed-form solution for surface deflections, which contains Kelvin Bessel functions, is used for fitting of measured deflections (Ioannides, 1990). The method that is based on four measured deflections is referred to as 'Best Fit 4', the one based on seven measured deflections as 'Best Fit 7' (Khazanovich *et al.*, 2001).

Depending on the number of deflection measurements used for the AREA method and the Best Fit method, respectively, the two methods deliver slightly different moduli of subgrade reaction (Khazanovich *et al.*, 2001). Multi-layered elastic simulations performed with the DIPLOMAT program (Khazanovich, 1994, Khazanovich and Ioannides, 1995) were the basis to recommend the 'Best Fit 4' method (using deflections measured in radial distances of 0, 305, 610, and 914 mm) for rigid pavements (Khazanovich *et al.*, 2001), see also (Hall *et al.*, 1997). Still, it is noteworthy that the 'Best Fit 4' method and the 'AREA7' method (integrating the deflection basin up to a radial distance of 1524 mm) are practically equivalent. Both methods deliver virtually the same back-calculated values of the modulus of subgrade reaction, see Figures 3 and 6 in (Khazanovich *et al.*, 2001). This provides the motivation to relate LASIX to directional variations of the deflection basin parameter AREA7.

3.3. Relation between LASIX and the coefficient of directional variation of AREA7 ('COVAREA7')

Standard FWD tests are nowadays evaluated by means of methods that are based on the assumption of an infinite

Table 10. Values of AREA7 [mm] obtained from the average of the three (to six) FWD tests performed along each of the eight directions for every one of the 10 slabs.

Slab #	Condition	N	NE	E	SE	S	SW	W	NW
A1-33354	Old	1122.93	1158.77	1189.41	1220.18	1180.95	1122.48	1015.41	1047.43
A1-33360	New	1107.20	1028.11	1010.01	1069.03	1065.66	1077.02	1053.67	1067.07
A1-33868	Old	1020.23	969.35	899.39	1015.66	1055.42	1078.83	1019.48	1004.60
A1-33873	New	985.27	969.70	942.21	973.16	1003.82	1005.12	978.44	958.00
A1-33874	Old	993.77	995.56	1026.19	1053.00	1020.13	1007.83	959.44	953.87
A2-47543	Old	1006.91	967.51	914.17	997.75	1043.41	1090.49	1049.67	1002.81
A2-50000	Old	1042.78	1046.65	1062.54	1136.01	1120.99	1106.30	986.85	976.25
A2-51995	New	931.31	947.22	927.77	948.69	932.44	902.20	846.59	856.10
A2-54003	Old	1123.93	1141.15	1128.28	1204.03	1168.86	1087.04	953.39	1011.14
A2-54440	New	928.54	924.48	893.49	947.75	931.07	923.58	878.11	881.74

plate, uniform subgrade stiffness, and, therefore, point-symmetric slab behaviour. However, multi-directional FWD testing underlined that rigid pavements which had been in service for a long time behave in a remarkable *asymmetric* fashion. Thus, back-analysing uniform slab properties from FWD tests could be questionable. In this context it is useful to categorise the asymmetric behaviour of slabs into ‘mild asymmetries’ and ‘strong asymmetries’. This is supported by LASIX, as will be demonstrated in the remainder of the present section.

The database shown in Appendix 1 contains the deflection measurements from 27 FWD tests performed on every one of the 10 tested slabs. For every slab, the following analysis is performed. The three (to six) deflections, measured by means of repeated testing in the same direction and at the same distance to the centre of the falling weight, are averaged. The deflection profile between the averaged deflections is approximated, in every direction, by means of a spline. It is integrated from the centre of the falling weight to a radial distance $R = 1524$ mm:

$$\text{AREA7} = \frac{1}{w_0} \int_0^R w(r) dr. \quad (5)$$

This yields one value of the AREA7 parameter for every measurement direction, see Table 10. These eight direction-dependent AREA7 values per slab are post-processed by computing their mean value, μ_{AREA7} , and their standard deviation, σ_{AREA7} , see Table 11. Dividing the latter by the former yields the coefficient of directional variation of the AREA7 values for every slab, which is referred to as COVAREA7. It is another measure for asymmetric slab behaviour.

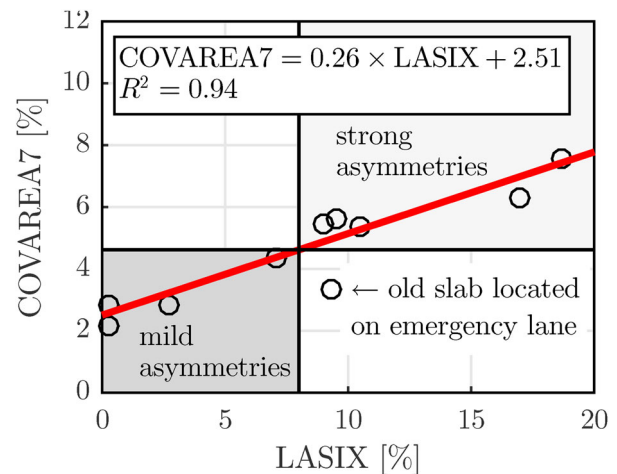
Table 11. Mean value, μ_{AREA7} , standard deviation, σ_{AREA7} , and coefficient of variation, COVAREA7, of the eight direction-dependent values of the AREA7 parameter of each slab.

Slab #	Condition	μ_{AREA7} [mm]	σ_{AREA7} [mm]	COVAREA7 [-]
A1-33354	Old	1132.19	70.81	6.25%
A1-33360	New	1059.72	29.85	2.82%
A1-33868	Old	1007.87	54.65	5.42%
A1-33873	New	976.97	21.45	2.20%
A1-33874	Old	1001.22	33.34	3.33%
A2-47543	Old	1009.09	53.93	5.34%
A2-50000	Old	1059.80	59.14	5.58%
A2-51995	New	911.54	39.86	4.37%
A2-54003	Old	1102.23	82.94	7.52%
A2-54440	New	913.59	25.61	2.80%

For all slabs except the *old* slab A1-33874, the \mathcal{A}_{28} -value of which amounts to 4.29%, see Table 6, which is *smaller* than the corresponding threshold value 5.2%, see Figure 4, the values of COVAREA7 from Table 11 are correlated with the values of LASIX from Table 7, see Figure 8. The quadratic correlation coefficient amounts to 94%.

Values of LASIX smaller than 8% refer to values of COVAREA7 smaller than 4.6%. Such coefficients of directional variation of the AREA7 parameter are representative for new slabs. They show only mild asymmetries resulting from their finite size and slab-to-slab interaction, while the stiffness of the subgrade can be expected to be uniform. Thus, it is realistic to identify a *uniform* modulus of subgrade reaction from deflections measured in driving direction, either by the Best Fit 4 method or the AREA7 method.

Values of LASIX larger than 8% refer, according to the red regression line in Figure 8, to values of COVAREA7 larger than 4.6%. Such coefficients of directional variation of the AREA7 values are representative for old slabs which show asymmetries because of directional degradation of the pavement structure, resulting from eccentric traffic loads. Whether or not the identification of *uniform* pavement properties,

**Figure 8.** Correlation between the coefficient of variation of the direction-dependent AREA7 values, COVAREA7, quantified based on results from multi-directional FWD testing over eight directions, and the Lateral Asymmetry Index LASIX according to Equation (1), related to T-shaped FWD testing; each symbol corresponds to one of the 10 tested slabs; the horizontal and vertical black lines represent the threshold values of COVAREA7 and LASIX distinguishing mild from strong asymmetries.

either by the Best Fit 4 method or the AREA7 method, is still realistic will be analysed in Section 3.4.

The exposure situation explains why COVAREA7 of the old slab A1-33874 amounts to 3.33%, see Table 11, which is smaller than the corresponding threshold value 4.6%. This slab was part of an emergency lane, see Table 1. Therefore, it was subjected to traffic loading only indirectly, namely, because of load transfer via tie bars connecting the tested slab to its neighbour which was part of the first lane and, therefore, directly exposed to traffic loads.

3.4. Variation of the modulus of subgrade reaction back-calculated from eight direction-specific values of AREA7 per slab

In the AREA method, the ‘dense-liquid’ model is used to back-calculate a uniform modulus of subgrade reaction from deflections measured in the driving direction. This model idealises the pavement structure as a plate (finite thickness, but infinite in-plane dimensions) resting on a Winkler foundation. Assuming that deflections measured in the driving direction are axisymmetric with respect to the axis of impact of the falling weight, the AREA parameter is translated into the radius of relative stiffness l_k (Ioannides *et al.*, 1989, Ioannides, 1990):

$$l_k \approx \left[\ln \left(\frac{\xi_1 - \text{AREA}}{\xi_2} \right) \times \frac{1}{\xi_3} \right]^{\xi_4}, \quad (6)$$

where ξ_1 , ξ_2 , ξ_3 , and ξ_4 are coefficients that depend on the specific AREA-parameter used, see (Hall *et al.*, 1997). The radius of relative stiffness, in turn, is equal to the fourth root of the bending stiffness of the plate, D , divided by the modulus of subgrade reaction, k , Westergaard (1926):

$$l_k = 4 \sqrt[4]{\frac{D}{k}}. \quad (7)$$

The values of D and k are usually optimised such that the model-simulated deflection basin reproduces the measured deflections in the best-possible fashion (Hall *et al.*, 1997, Khasanovich *et al.*, 2001). Therefore, D is not necessarily equal to the bending stiffness of the concrete slab.

If measured deflections are direction-dependent (= asymmetric), the assumption of a point-symmetric deflection basin is only useful, provided that direction-dependent values of the AREA parameter are translated, by means of Equations (6) and (7), into virtually the same value of k . Whether or not this is the case, will be checked in the following.

For every slab, the following two-step procedure is performed. Step 1: The eight direction-dependent values of AREA7, see Table 10, are translated by means of Equation (6) into eight corresponding values of l_k . Given that the AREA7-parameter is expressed in millimetres, the corresponding values of the empirical ξ -constants read as $\xi_1 = 1524$, $\xi_2 = 7358.59$, $\xi_3 = -0.197868$, $\xi_4 = 2.566$, see (Hall *et al.*, 1997) for details. With these values, Equation (6) yields values of l_k in millimetres. Step 2: The eight direction-dependent values of l_k are translated by means of Equation (7) into eight corresponding values of k . Thereby, the plate stiffness D is set equal to D_s which denotes the bending

stiffness of the concrete slabs (other choices for D will be discussed at the end of the Section):

$$D_s = \frac{E_c h_s^3}{12(1 - \nu_c^2)}, \quad (8)$$

where E_c denotes the modulus of elasticity of concrete, h_s the thickness of the slab, and ν_c Poisson’s ratio of concrete. Herein, these quantities are equal to 36500 MPa, 0.22 m, and 0.2, respectively, see also (Díaz Flores *et al.*, 2021). Inserting these values into Equation (8) yields

$$D_s = 33.74 \text{ MPa m}^3. \quad (9)$$

An expression for corresponding values of k is obtained by solving Equation (7) for k :

$$k = \frac{D_s}{(l_k)^4}. \quad (10)$$

This completes Step 2.

Applying the procedure described in the preceding paragraph to eight direction-dependent values of AREA7 per slab, allows for computing eight k -values per slab. They are the basis for computing slab-specific mean values of k , denoted as μ_k , as well as corresponding standard deviations, σ_k , and coefficients of variation, $CV(k) = \sigma_k / \mu_k$, see Table 12. The

Table 12. Mean value, μ_k , standard deviation, σ_k , and coefficient of variation, $CV(k)$, of the eight direction-dependent values of the modulus of subgrade reaction k of each slab.

Slab #	Condition	μ_k [MPa/mm]	σ_k [MPa/mm]	$CV(k)$ [-]
A1-33354	Old	0.0374	0.0249	66.58%
A1-33360	New	0.0609	0.0148	24.33%
A1-33868	Old	0.0950	0.0437	45.97%
A1-33873	New	0.1128	0.0175	15.55%
A1-33874	Old	0.0957	0.0237	24.77%
A2-47543	Old	0.0937	0.0392	41.86%
A2-50000	Old	0.0646	0.0303	46.88%
A2-51995	New	0.1814	0.0522	28.77%
A2-54003	Old	0.0505	0.0395	78.05%
A2-54440	New	0.1759	0.0309	17.57%

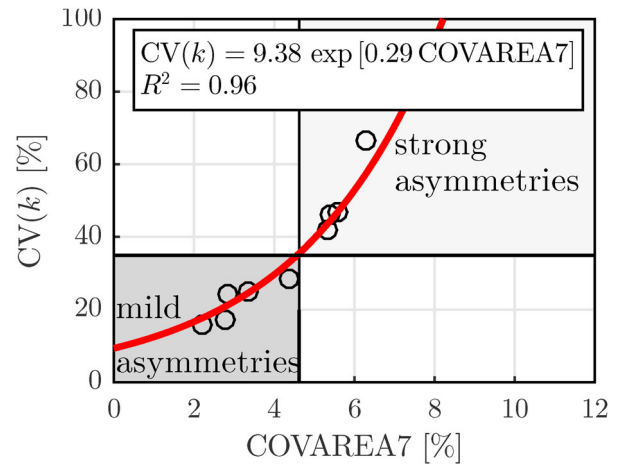


Figure 9. Correlation between the coefficient of variation of eight values of the modulus of subgrade reaction, back-calculated from eight direction-dependent AREA7 values per slab, see $CV(k)$ in Table 12, and COVAREA7, see Table 11; each symbol corresponds to one of the 10 tested slabs; the horizontal and vertical black lines represent threshold values separating mild from strong asymmetries.

10 slab-specific values of $CV(k)$ are finally correlated with the corresponding values of COVAREA7 from Table 10, see Figure 9.

For pavement structures exhibiting mild asymmetries, as expressed by COVAREA7-values smaller than 4.6%, values of $CV(k)$ smaller than 35% are found. In such cases, the assumptions of a *point-symmetric* deflection basin and a *uniform* modulus of subgrade reaction appear to be useful for engineering purposes. For pavement structures exhibiting strong asymmetries, as expressed by COVAREA7-values larger than 4.6%, values of $CV(k)$ larger than 35% are found. In such cases, the assumptions of a *point-symmetric* deflection basin and *uniform* pavement properties are questionable.

Finally, it is shown that the values of $CV(k)$ listed in Table 12 and illustrated in Figure 9 are independent of the specific choice for the plate stiffness D in Equation (7). Above, the specific choice $D = D_s$ was made. This provides the motivation to multiply D_s by a slab-specific scaling factor α_s . In order to analyse the corresponding implications on k , both sides of Equation (10) are multiplied by α_s :

$$\alpha_s k = \frac{\alpha_s D_s}{(l_k)^4}. \quad (11)$$

Equation (11) underlines that scaling of D_s by a factor α_s leads to k -values scaled by the same factor α_s . Scaling of the eight k -values per slab by a factor of α_s , in turn, leads to mean values μ_k and standard deviations σ_k scaled by the same factor α_s . In other words, both the μ_k -values and σ_k -values in Table 12 are to be multiplied by α_s . This underlines that the coefficient of variation, $CV(k) = \sigma_k / \mu_k$, is independent of α_s . It is concluded that the last column in Table 12 and the ordinate values in Figure 9 remain the same, even if D is optimised in order to reproduce the measured deflections (rather than setting it equal to D_s).

3.5. Limitations and future outlook

The here-analysed FWD experiments were carried out on slabs made from normal concrete, with a thickness of 0.22 m, lengths ranging from 4.50 m to 5.60 m, widths from 3.10 m to 4.20 m, and length-to-width ratios from 1.12 to 1.81. The optimal value of c and the threshold values of LASIX, A_{28} , COVAREA7, and $CV(k)$ refer to slabs with properties listed above. Otherwise, these values are questionable. In the case of bonded white-toppings featuring square slabs 1.80 m long and wide, for instance, even a new radial distance c of the lateral geophones from the centre of the slabs would need to be optimised.

All non-standard FWD tests performed so far included multi-directional measurements of surface deflections. A prototype for FWD testing with a T-shaped arrangement of the geophones is in its design phase. This testing device will reduce the in-situ efforts to those known from standard FWD testing: piloting the FWD trailer to the slab of interest, lowering the impact transducer and the geophones onto the surface of the slab, lifting and dropping the falling weight while recording the surface deflections, uplifting the impact transducer and

the geophones, and piloting the FWD trailer to the next slab of interest.

4. Conclusions

An optimal T-shaped arrangement of nine geophones was developed: one at the centre of impact (= centre of the slab), six along the driving direction, one right and one left of the centre. The following conclusions are drawn:

- As for central FWD testing with a T-shaped arrangement of geophones, the optimal distance of the lateral geophones from the centre of impact is equal to 1.20 m.
- It is possible to integrate the proposed arrangement (or an alternative similar to it) into trailers complying with the maximum allowed widths of vehicles, e.g. 2.44 m in the USA, 2.55 m in China, and 2.60 m in Europe.
- This renders highly automated and, therefore, rapid FWD testing feasible, with on-site efforts equal to those known from standard FWD testing.
- State-of-the-art evaluation of deflections measured in driving direction remains possible, as long as a suitable amount of geophones remain arranged along the driving direction (here: seven including the one at the centre of the falling weight).
- The 'Lateral Asymmetry Index' (LASIX) is a deflection-basin-parameter customised for T-shaped FWD testing. It enables the quantification of asymmetric slab behaviour.
- Values of LASIX smaller than 8% refer to coefficients of directional variation of AREA7 smaller than 4.6%. For slabs presenting geometric and stiffness properties within the intervals studied, such values are representative for new slabs which show only mild asymmetries. The latter result from their finite size and slab-to-slab interaction, while the stiffness of the subgrade can be expected to be uniform. Thus, it is realistic to identify a *uniform* modulus of subgrade reaction, either by the Best Fit 4 method or the AREA7 method.
- Values of LASIX larger than 8% refer to coefficients of directional variation of AREA7 larger than 4.6%. For slabs presenting geometric and stiffness properties within the intervals studied, such values are representative for old slabs with directional degradation of the pavement structure, resulting from eccentric traffic loads. Thus, it is questionable to identify *uniform* properties of the pavement structure.

In the future, it will be interesting

- to integrate central FWD tests with a T-shaped arrangement of geophones into the monitoring strategy of pavement slabs made of concrete, i.e. to perform such tests regularly on specific slabs in order to study the evolution of LASIX as a function of the age of the slab and of the service loads to which it is exposed (traffic and hygro-thermal loads), and
- to perform such tests on slabs with different sizes and stiffness properties, in order to widen their range of applicability.

List of symbols

a	length of the slab
A_{28}	Effective asymmetry index
b	width of the slab
c	optimal radial distance of the lateral geophones from the centre of the slab
$CV(k)$	coefficient of variation of the modulus of subgrade reaction
d	direction
D	Bending stiffness of the plate of the 'dense-liquid' model
D_s	Bending stiffness of the tested concrete slabs
E	East
E_c	modulus of elasticity of concrete
g	geophones
h_s	thickness of the slab
i	Test number
j	Summation index for all 28 possible combinations of directions compared in $A_{d,\delta}$
k	modulus of subgrade reaction of the Winkler foundation of the 'dense-liquid' model
k_r	radius of relative stiffness
ℓ	radial length of integration in Equation (3)
N	North
NE	Northeast
NW	Northwest
r	radial coordinate
$r_{d,g}$	radial coordinate of geophone g measuring deflections in the direction d
R^2	coefficient of determination
S	South
SE	Southeast
SW	Southwest
$w(r)$	deflection at the radial distance r from the centre of the slab
$w_d(r=0)$	deflection at the radial distance $r=0$ from the centre of the slab measured in direction d
$w_\delta(r=0)$	deflection at the radial distance $r=0$ from the centre of the slab measured in direction δ
$w_d(r)$	deflection at the radial distance r from the centre of the slab measured in direction d
$w_\delta(r)$	deflection at the radial distance r from the centre of the slab measured in direction δ
$w_E(r=c)$	deflection at the radial distance $r=c$ from the centre of the slab measured in the direction E
w_γ	deflection measured by the geophone at the radial distance of $r = \gamma \Delta r$, where $\gamma = 0, 1, 2, \text{ or } 3$
$w_{int}(r)$	spline-interpolated deflection at the radial distance r
$w_m(r)$	measured deflection at the radial distance r
$w_N(r=c)$	deflection at the radial distance $r=c$ from the centre of the slab measured in the direction N
$w_W(r=c)$	deflection at the radial distance $r=c$ from the centre of the slab measured in the direction W
W	West
γ	geophone number to which the deflection w_γ corresponds, see Equation (4)
δ	in $A_{d,\delta}$, direction against which the direction d is compared, $d \neq \delta$
Δr	uniform distance between two neighbouring geophones
μ_{AREA7}	mean value of all eight AREA7 values per slab
ν_c	Poisson's ratio of concrete
ξ_i	empirical coefficients, with $i = 1, 2, 3, 4$
σ_{AREA7}	standard deviation of all eight AREA7 values per slab
φ_d	polar angle of the direction d

List of abbreviations

AREA4	AREA value based on four measured deflections
AREA7	AREA value based on seven measured deflections
Best fit 4	best fit method based on four measured deflections
Best fit 7	best fit method based on seven measured deflections
COVAREA7	coefficient of directional variation of AREA7
FWD	Falling Weight Deflectometer
LASIX	Lateral asymmetry index

Acknowledgments

The help of Pia Mandahus (TU Wien, Vienna, Austria), Marek Milcevic, Roman Oblak and Harald Aigner (Nievelt Labor GmbH, Höbersdorf, Austria) as well as interesting discussions with Wolfgang Kluger-Eigl (TU Wien), Martin Peyerl and Gerald Maier (Smart Minerals GmbH, Vienna, Austria) as well as Reinhard Lohmann-Pichler and Karl Gragger (ASFINAG Bau Management GmbH) are gratefully acknowledged.

Disclosure statement

No potential conflict of interest was reported by the author(s).

Funding

This research received financial support by the Austrian Research Promotion Agency (FFG), the Austrian Ministry for Transport and Technology (bmvit), ÖBB-Infrastruktur AG (Vienna, Austria), and ASFINAG Bau Management GmbH (Vienna, Austria), within VIF-project 2015 'STRUKTurelle Zustandserhebung und -bewertung von Betondecke (CONcrete) auf Projektebene - ConSTRUKT' and the Bridge Project 2021 'Grundlegende Analyse von FWD-Versuchen: innovative Experimente, moderne Struktursimulationen, statistische Datenanalyse - FALL-INGweight'. The authors also acknowledge the TU Wien University Library for financial support through its Open Access Funding Programme.

ORCID

Rodrigo Díaz Flores  <http://orcid.org/0000-0002-1153-9875>
 Mehdi Aminbaghai  <http://orcid.org/0000-0002-8302-6024>
 Lukas Eberhardsteiner  <http://orcid.org/0000-0003-2153-9315>
 Bernhard L. A. Pichler  <http://orcid.org/0000-0002-6468-1840>

References

- AASHTO, 2008. Mechanistic-Empirical Pavement Design Guide: A Manual of Practice. In: *American Association of State Highway and Transportation Officials*. Washington, D.C.
- Bay, J., Stokoe II, K., and Jackson, J., 1995. Development and preliminary investigation of rolling dynamic deflectometer. *Transportation Research Record*, 1473, 43–54.
- Briggs, R.C., et al. 2000. A comparison of the rolling weight deflectometer with the falling weight deflectometer. In: *Nondestructive Testing of Pavements and Backcalculation of Moduli: Third Volume*. ASTM STP 1375.
- Coni, M., et al. 2021. Fast falling weight deflectometer method for condition assessment of RC bridges. *Applied Sciences*, 11 (4), 1743.
- Darter, M.I., Hall, K.T., and Kuo, C.M., 1995. *Support under Portland cement concrete pavements*. National Cooperative Highway Research Program, Project 1-30 FY'93.
- Díaz Flores, R., et al. 2021. Multi-directional falling weight deflectometer (FWD) testing and quantification of the effective modulus of subgrade reaction for concrete roads. *International Journal of Pavement Engineering*, 1–19. doi:10.1080/10298436.2021.2006651.
- Fleming, P.R., Frost, M.W., and Lambert, J.P., 2007. Review of lightweight deflectometer for routine in situ assessment of pavement material stiffness. *Transportation Research Record*, 2004 (1), 80–87.
- Hall, K.T., and Mohseni, A., 1991. Backcalculation of asphalt concrete-overlaid portland cement concrete pavement layer moduli. *Transportation Research Record*, 1293, 112–123.
- Hall, K.T., et al. 1997. *LTPP data analysis. phase I: Validation of guidelines for k-value selection and concrete pavement performance prediction*. Federal Highway Administration, No. FHWA-RD-96-198.
- Hoffman, M.S., and Thompson, M., 1980. *Mechanistic interpretation of nondestructive pavement testing deflections*. University of Illinois at Urbana-Champaign, FHWA/IL/UI-190.

- Ioannides, A.M., 1990. Dimensional analysis in NDT rigid pavement evaluation. *Journal of Transportation Engineering*, 116 (1), 23–36.
- Ioannides, A., Barenberg, E., and Lary, J., 1989. Interpretation of falling weight deflectometer results using principles of dimensional analysis. *In: Proceedings, 4th International Conference on Concrete Pavement Design and Rehabilitation, Purdue University*. 231–247.
- Ioannides, A.M., and Khazanovich, L., 1998. Nonlinear temperature effects on multilayered concrete pavements. *Journal of Transportation Engineering*, 124 (2), 128–136.
- Khazanovich, L., 1994. *Structural analysis of multi-layered concrete pavement systems*. Thesis (PhD). University of Illinois at Urbana-Champaign.
- Khazanovich, L., and Ioannides, A.M., 1995. DIPLOMAT: analysis program for bituminous and concrete pavements. *Transportation Research Record*, 1482, 52–60.
- Khazanovich, L., Tayabji, S.D., and Darter, M.I., 2001. *Backcalculation of layer parameters for performance for LTPP test sections, volume I: Slab on elastic solid and slab on dense-liquid foundation analysis of rigid pavements*. United States. Federal Highway Administration. Office of Engineering.
- Losberg, A., 1960. *Structurally reinforced concrete pavements*. (Vol. 29), Akademiforlaget Gumperts.
- Nazzal, M.D., et al. 2007. Evaluating the light falling weight deflectometer device for in situ measurement of elastic modulus of pavement layers. *Transportation Research Record*, 2016 (1), 13–22.
- Packard, R.G., 1984. *Thickness design for concrete highway and street pavements*. Portland Cement Association.
- Packard, R.G., and Tayabji, S.D., 1985. New PCA thickness design procedure for concrete highway and street pavements. *In: Third International Conference on Concrete Pavement Design and Rehabilitation*, West Lafayette. Purdue University.
- Pratelli, C., et al. 2018. Preliminary in-situ evaluation of an innovative, semi-flexible pavement wearing course mixture using fast falling weight deflectometer. *Materials*, 11 (4), 611.
- Smith, K.D., et al. 2017. *Using Falling Weight Deflectometer Data with Mechanistic-Empirical Design and Analysis, Volume I*. Federal Highway Administration, United States, FHWA-HRT-16-009.
- Westergaard, H.M., 1926. *Stresses in concrete pavements computed by theoretical analysis*. Public roads.
- Winkler, E., 1867. *Die Lehre von der Elasticität und Festigkeit mit besonderer Rücksicht auf ihre Anwendung in der Technik [lessons on elasticity and strength of materials with special consideration of their application in technology]*. H. Dominicus, Prague.

Appendix

Appendix 1. Results of multi-directional FWD testing of all slabs

Table A1. Maximum deflections measured during the 27 FWD tests performed on the old slab A1-33354 [mm].

Test Direction	Test Number	Geophone								
		$g=1$	$g=2$	$g=3$	$g=4$	$g=5$	$g=6$	$g=7$	$g=8$	$g=9$
$d=1$ (N)	$i=1$	0.346	0.313	0.304	0.281	0.240	0.201	0.164	0.136	0.104
$d=1$ (N)	$i=2$	0.334	0.307	0.296	0.273	0.234	0.196	0.159	0.134	0.102
$d=1$ (N)	$i=3$	0.333	0.305	0.295	0.272	0.233	0.195	0.159	0.131	0.102
$d=2$ (NE)	$i=1$	0.342	0.311	0.302	0.283	0.247	0.209	0.171	0.138	0.105
$d=2$ (NE)	$i=2$	0.339	0.310	0.305	0.284	0.246	0.209	0.169	0.136	0.104
$d=2$ (NE)	$i=3$	0.336	0.310	0.304	0.284	0.247	0.209	0.170	0.137	0.105
$d=3$ (E)	$i=1$	0.339	0.318	0.311	0.291	0.258	0.217	0.172	0.135	0.104
$d=3$ (E)	$i=2$	0.339	0.316	0.310	0.290	0.257	0.216	0.171	0.134	0.104
$d=3$ (E)	$i=3$	0.337	0.315	0.309	0.289	0.256	0.215	0.171	0.133	0.104
$d=4$ (SE)	$i=1$	0.334	0.301	0.296	0.273	0.241	0.206	0.171	0.138	0.106
$d=4$ (SE)	$i=2$	0.335	0.303	0.296	0.274	0.243	0.208	0.171	0.139	0.105
$d=4$ (SE)	$i=3$	0.335	0.303	0.296	0.277	0.246	0.209	0.173	0.139	0.106
$d=5$ (S)	$i=1$	0.329	0.303	0.296	0.275	0.245	0.212	0.177	0.145	0.114
$d=5$ (S)	$i=2$	0.329	0.304	0.296	0.277	0.246	0.212	0.176	0.145	0.114
$d=5$ (S)	$i=3$	0.330	0.304	0.295	0.277	0.246	0.212	0.177	0.145	0.114
$d=6$ (SW)	$i=1$	0.329	0.278	0.267	0.245	0.209	0.175	0.142	0.114	0.091
$d=6$ (SW)	$i=2$	0.325	0.266	0.265	0.244	0.207	0.173	0.140	0.113	0.088
$d=6$ (SW)	$i=3$	0.327	0.271	0.266	0.244	0.208	0.174	0.142	0.113	0.089
$d=7$ (W)	$i=1$	0.327	0.275	0.263	0.237	0.196	0.160	0.130	0.110	
$d=7$ (W)	$i=2$	0.325	0.275	0.266	0.237	0.196	0.160	0.130	0.108	
$d=7$ (W)	$i=3$	0.325	0.274	0.262	0.236	0.194	0.159	0.128	0.106	
$d=8$ (NW)	$i=1$	0.329	0.286	0.270	0.247	0.207	0.171	0.139	0.115	0.091
$d=8$ (NW)	$i=2$	0.328	0.284	0.270	0.246	0.206	0.171	0.138	0.115	0.093
$d=8$ (NW)	$i=3$	0.328	0.283	0.270	0.245	0.206	0.170	0.138	0.114	0.093
$d=1$ (N)	$i=4$	0.329	0.302	0.288	0.266	0.228	0.188	0.151	0.120	0.093
$d=1$ (N)	$i=5$	0.326	0.298	0.285	0.262	0.225	0.185	0.150	0.120	0.094
$d=1$ (N)	$i=6$	0.328	0.298	0.286	0.263	0.226	0.187	0.152	0.123	0.095

Table A2. Maximum deflections measured during the 27 FWD tests performed on the new slab A1-33360 [mm].

Test Direction	Test Number	Geophone								
		$g=1$	$g=2$	$g=3$	$g=4$	$g=5$	$g=6$	$g=7$	$g=8$	$g=9$
$d=1$ (N)	$i=1$	0.257	0.228	0.219	0.202	0.176	0.152	0.129	0.112	0.093
$d=1$ (N)	$i=2$	0.259	0.229	0.221	0.203	0.178	0.153	0.129	0.112	0.093
$d=1$ (N)	$i=3$	0.256	0.227	0.219	0.201	0.175	0.152	0.129	0.110	0.090
$d=2$ (NE)	$i=1$	0.264	0.219	0.208	0.184	0.163	0.140	0.119	0.102	0.088
$d=2$ (NE)	$i=2$	0.260	0.216	0.206	0.189	0.162	0.138	0.118	0.097	0.082
$d=2$ (NE)	$i=3$	0.261	0.216	0.206	0.190	0.161	0.138	0.117	0.097	0.082
$d=3$ (E)	$i=1$	0.266	0.222	0.209	0.191	0.153	0.136	0.113	0.096	0.079
$d=3$ (E)	$i=2$	0.259	0.214	0.204	0.185	0.156	0.132	0.110	0.094	0.080
$d=3$ (E)	$i=3$	0.261	0.217	0.203	0.186	0.156	0.132	0.109	0.092	0.076
$d=4$ (SE)	$i=1$	0.258	0.206	0.203	0.182	0.152	0.126	0.100	0.093	0.078
$d=4$ (SE)	$i=2$	0.256	0.211	0.201	0.181	0.151	0.125	0.102	0.092	0.080
$d=4$ (SE)	$i=3$	0.256	0.213	0.198	0.179	0.151	0.126	0.102	0.093	0.085
$d=5$ (S)	$i=1$	0.261	0.231	0.218	0.198	0.165	0.142	0.118	0.096	0.086
$d=5$ (S)	$i=2$	0.259	0.229	0.214	0.197	0.166	0.141	0.117	0.096	0.085
$d=5$ (S)	$i=3$	0.261	0.230	0.215	0.197	0.169	0.141	0.117	0.097	0.085
$d=6$ (SW)	$i=1$	0.262	0.217	0.198	0.192	0.151	0.123	0.104	0.087	0.074
$d=6$ (SW)	$i=2$	0.260	0.216	0.195	0.190	0.149	0.121	0.105	0.085	0.073
$d=6$ (SW)	$i=3$	0.260	0.216	0.198	0.189	0.150	0.122	0.105	0.086	0.073
$d=7$ (W)	$i=1$	0.259	0.230	0.219	0.199	0.162	0.132	0.108	0.090	
$d=7$ (W)	$i=2$	0.260	0.231	0.220	0.200	0.163	0.133	0.104	0.091	
$d=7$ (W)	$i=3$	0.259	0.229	0.218	0.198	0.162	0.133	0.106	0.091	
$d=8$ (NW)	$i=1$	0.260	0.229	0.215	0.199	0.161	0.142	0.117	0.098	0.082
$d=8$ (NW)	$i=2$	0.259	0.228	0.217	0.198	0.168	0.142	0.118	0.099	0.082
$d=8$ (NW)	$i=3$	0.260	0.227	0.214	0.199	0.169	0.143	0.118	0.100	0.085
$d=1$ (N)	$i=4$	0.258	0.231	0.216	0.196	0.174	0.152	0.130	0.112	0.096
$d=1$ (N)	$i=5$	0.260	0.229	0.218	0.200	0.175	0.151	0.130	0.109	0.093
$d=1$ (N)	$i=6$	0.259	0.229	0.217	0.200	0.174	0.151	0.130	0.109	0.094

Table A3. Maximum deflections measured during the 27 FWD tests performed on the old slab A1-33868 [mm].

Test Direction	Test Number	Geophone								
		$g=1$	$g=2$	$g=3$	$g=4$	$g=5$	$g=6$	$g=7$	$g=8$	$g=9$
$d=1$ (N)	$i=1$	0.322	0.295	0.274	0.246	0.203	0.157	0.114	0.081	0.057
$d=1$ (N)	$i=2$	0.329	0.292	0.277	0.250	0.204	0.155	0.114	0.079	0.052
$d=1$ (N)	$i=3$	0.329	0.292	0.275	0.246	0.204	0.159	0.114	0.084	0.059
$d=2$ (NE)	$i=1$	0.321	0.279	0.263	0.234	0.182	0.138	0.099	0.070	0.052
$d=2$ (NE)	$i=2$	0.326	0.280	0.266	0.235	0.183	0.137	0.099	0.070	0.046
$d=2$ (NE)	$i=3$	0.327	0.281	0.262	0.233	0.183	0.135	0.099	0.070	0.048
$d=3$ (E)	$i=1$	0.324	0.274	0.252	0.218	0.160	0.116	0.082		
$d=3$ (E)	$i=2$	0.323	0.268	0.250	0.216	0.159	0.115	0.080		
$d=3$ (E)	$i=3$	0.322	0.270	0.250	0.216	0.159	0.114	0.079		
$d=4$ (SE)	$i=1$	0.320	0.260	0.243	0.217	0.167	0.124	0.090	0.066	0.045
$d=4$ (SE)	$i=2$	0.320	0.265	0.244	0.214	0.168	0.124	0.089	0.065	0.044
$d=4$ (SE)	$i=3$	0.320	0.264	0.245	0.216	0.168	0.124	0.090	0.064	0.044
$d=5$ (S)	$i=1$	0.322	0.288	0.273	0.250	0.205	0.164	0.121	0.088	0.062
$d=5$ (S)	$i=2$	0.319	0.286	0.272	0.248	0.202	0.161	0.119	0.089	0.063
$d=5$ (S)	$i=3$	0.318	0.286	0.269	0.248	0.203	0.160	0.119	0.087	0.060
$d=6$ (SW)	$i=1$	0.318	0.272	0.257	0.232	0.184	0.142	0.104	0.074	0.050
$d=6$ (SW)	$i=2$	0.317	0.269	0.255	0.230	0.182	0.142	0.104	0.073	0.049
$d=6$ (SW)	$i=3$	0.317	0.270	0.255	0.230	0.182	0.142	0.104	0.073	0.049
$d=7$ (W)	$i=1$	0.319	0.284	0.274	0.247	0.194	0.144	0.099	0.067	
$d=7$ (W)	$i=2$	0.318	0.282	0.273	0.245	0.193	0.144	0.099	0.067	
$d=7$ (W)	$i=3$	0.321	0.283	0.275	0.247	0.195	0.145	0.101	0.064	
$d=8$ (NW)	$i=1$	0.314	0.274	0.261	0.236	0.189	0.141	0.102	0.073	0.046
$d=8$ (NW)	$i=2$	0.315	0.274	0.265	0.236	0.189	0.141	0.102	0.073	0.050
$d=8$ (NW)	$i=3$	0.315	0.274	0.261	0.237	0.189	0.141	0.102	0.073	0.049
$d=1$ (N)	$i=4$	0.317	0.276	0.262	0.235	0.188	0.146	0.108	0.078	0.053
$d=1$ (N)	$i=5$	0.317	0.278	0.260	0.235	0.189	0.146	0.108	0.076	0.053
$d=1$ (N)	$i=6$	0.317	0.277	0.263	0.235	0.188	0.147	0.108	0.077	0.054

Table A4. Maximum deflections measured during the 27 FWD tests performed on the new slab A1-33873 [mm].

Test Direction	Test Number	Geophone								
		$g=1$	$g=2$	$g=3$	$g=4$	$g=5$	$g=6$	$g=7$	$g=8$	$g=9$
$d=1$ (N)	$i=1$	0.159	0.125	0.119	0.107	0.091	0.075	0.061	0.051	0.041
$d=1$ (N)	$i=2$	0.153	0.123	0.117	0.105	0.091	0.074	0.061	0.049	0.041
$d=1$ (N)	$i=3$	0.152	0.123	0.115	0.104	0.088	0.073	0.060	0.048	0.039
$d=2$ (NE)	$i=1$	0.152	0.122	0.119	0.104	0.086	0.071	0.058	0.046	0.036
$d=2$ (NE)	$i=2$	0.150	0.122	0.115	0.102	0.086	0.071	0.056	0.043	0.035
$d=2$ (NE)	$i=3$	0.151	0.122	0.115	0.102	0.086	0.071	0.056	0.044	0.033
$d=3$ (E)	$i=1$	0.152	0.120	0.112	0.102	0.083	0.068	0.051		
$d=3$ (E)	$i=2$	0.150	0.119	0.112	0.101	0.083	0.068	0.050		
$d=3$ (E)	$i=3$	0.150	0.118	0.113	0.102	0.083	0.068	0.051		
$d=4$ (SE)	$i=1$	0.152	0.112	0.111	0.097	0.076	0.063	0.051	0.040	0.030
$d=4$ (SE)	$i=2$	0.151	0.111	0.104	0.094	0.075	0.063	0.049	0.037	0.029
$d=4$ (SE)	$i=3$	0.152	0.112	0.104	0.096	0.078	0.064	0.049	0.039	0.031
$d=5$ (S)	$i=1$	0.150	0.125	0.115	0.106	0.091	0.072	0.056	0.047	0.037
$d=5$ (S)	$i=2$	0.148	0.121	0.117	0.108	0.091	0.071	0.059	0.047	0.037
$d=5$ (S)	$i=3$	0.149	0.123	0.116	0.108	0.090	0.071	0.059	0.047	0.039
$d=6$ (SW)	$i=1$	0.149	0.112	0.106	0.095	0.079	0.065	0.052	0.044	0.038
$d=6$ (SW)	$i=2$	0.147	0.110	0.106	0.095	0.079	0.067	0.052	0.044	0.038
$d=6$ (SW)	$i=3$	0.147	0.110	0.106	0.095	0.079	0.067	0.052	0.044	0.038
$d=7$ (W)	$i=1$	0.148	0.123	0.117	0.105	0.084	0.068	0.055	0.044	
$d=7$ (W)	$i=2$	0.149	0.123	0.115	0.105	0.083	0.068	0.054	0.044	
$d=7$ (W)	$i=3$	0.149	0.124	0.117	0.105	0.085	0.068	0.055	0.044	
$d=8$ (NW)	$i=1$	0.148	0.118	0.113	0.101	0.083	0.068	0.053	0.043	0.033
$d=8$ (NW)	$i=2$	0.148	0.118	0.113	0.101	0.083	0.067	0.053	0.043	0.032
$d=8$ (NW)	$i=3$	0.149	0.121	0.109	0.101	0.084	0.067	0.055	0.043	0.033
$d=1$ (N)	$i=4$	0.148	0.120	0.115	0.104	0.086	0.072	0.059	0.049	0.037
$d=1$ (N)	$i=5$	0.148	0.122	0.115	0.103	0.087	0.073	0.059	0.047	0.038
$d=1$ (N)	$i=6$	0.149	0.122	0.116	0.106	0.088	0.074	0.060	0.043	0.039

Table A5. Maximum deflections measured during the 27 FWD tests performed on the old slab A1-33874 [mm].

Test Direction	Test Number	Geophone								
		$g=1$	$g=2$	$g=3$	$g=4$	$g=5$	$g=6$	$g=7$	$g=8$	$g=9$
$d=1$ (N)	$i=1$	0.204	0.174	0.159	0.145	0.119	0.096	0.077	0.063	0.048
$d=1$ (N)	$i=2$	0.205	0.174	0.163	0.147	0.121	0.098	0.079	0.061	0.050
$d=1$ (N)	$i=3$	0.204	0.174	0.162	0.146	0.119	0.096	0.077	0.059	0.047
$d=2$ (NE)	$i=1$	0.200	0.168	0.159	0.143	0.119	0.098	0.079	0.066	0.050
$d=2$ (NE)	$i=2$	0.203	0.171	0.158	0.142	0.118	0.099	0.080	0.067	0.052
$d=2$ (NE)	$i=3$	0.204	0.173	0.159	0.141	0.118	0.097	0.080	0.066	0.052
$d=3$ (E)	$i=1$	0.198	0.169	0.159	0.142	0.120	0.103	0.089		
$d=3$ (E)	$i=2$	0.202	0.173	0.159	0.144	0.123	0.107	0.092		
$d=3$ (E)	$i=3$	0.206	0.172	0.161	0.144	0.123	0.107	0.091		
$d=4$ (SE)	$i=1$	0.205	0.169	0.152	0.141	0.116	0.095	0.075	0.061	0.048
$d=4$ (SE)	$i=2$	0.205	0.165	0.155	0.140	0.113	0.093	0.074	0.060	0.048
$d=4$ (SE)	$i=3$	0.204	0.170	0.153	0.140	0.115	0.093	0.074	0.060	0.048
$d=5$ (S)	$i=1$	0.203	0.179	0.171	0.151	0.127	0.099	0.076	0.059	0.045
$d=5$ (S)	$i=2$	0.204	0.185	0.168	0.150	0.117	0.098	0.076	0.059	0.046
$d=5$ (S)	$i=3$	0.204	0.183	0.169	0.151	0.113	0.097	0.076	0.059	0.045
$d=6$ (SW)	$i=1$	0.200	0.160	0.145	0.131	0.105	0.081	0.061	0.047	0.035
$d=6$ (SW)	$i=2$	0.201	0.161	0.147	0.132	0.105	0.081	0.061	0.047	0.033
$d=6$ (SW)	$i=3$	0.202	0.161	0.148	0.133	0.106	0.081	0.061	0.047	0.035
$d=7$ (W)	$i=1$	0.205	0.172	0.167	0.144	0.112	0.089	0.066	0.048	
$d=7$ (W)	$i=2$	0.201	0.173	0.156	0.139	0.112	0.085	0.065	0.048	
$d=7$ (W)	$i=3$	0.202	0.173	0.158	0.140	0.112	0.086	0.066	0.048	
$d=8$ (NW)	$i=1$	0.201	0.166	0.152	0.136	0.111	0.089	0.069	0.053	0.041
$d=8$ (NW)	$i=2$	0.203	0.168	0.152	0.137	0.112	0.089	0.069	0.054	0.041
$d=8$ (NW)	$i=3$	0.203	0.168	0.154	0.137	0.112	0.089	0.070	0.054	0.041
$d=1$ (N)	$i=4$	0.203	0.172	0.161	0.144	0.118	0.096	0.077	0.061	0.047
$d=1$ (N)	$i=5$	0.204	0.174	0.159	0.143	0.119	0.096	0.077	0.064	0.048
$d=1$ (N)	$i=6$	0.205	0.175	0.158	0.142	0.119	0.096	0.077	0.064	0.049

Table A6. Maximum deflections measured during the 27 FWD tests performed on the old slab A2-47543 [mm].

Test Direction	Test Number	Geophone								
		<i>g</i> = 1	<i>g</i> = 2	<i>g</i> = 3	<i>g</i> = 4	<i>g</i> = 5	<i>g</i> = 6	<i>g</i> = 7	<i>g</i> = 8	<i>g</i> = 9
<i>d</i> = 1 (N)	<i>i</i> = 1	0.389	0.338	0.319	0.285	0.233	0.183	0.139	0.103	0.075
<i>d</i> = 1 (N)	<i>i</i> = 2	0.384	0.333	0.316	0.283	0.230	0.181	0.137	0.102	0.070
<i>d</i> = 1 (N)	<i>i</i> = 3	0.381	0.329	0.312	0.279	0.227	0.178	0.135	0.099	0.070
<i>d</i> = 2 (NE)	<i>i</i> = 1	0.371	0.323	0.295	0.263	0.205	0.157	0.117	0.082	0.059
<i>d</i> = 2 (NE)	<i>i</i> = 2	0.372	0.323	0.298	0.264	0.206	0.158	0.118	0.082	0.061
<i>d</i> = 2 (NE)	<i>i</i> = 3	0.372	0.323	0.298	0.264	0.207	0.159	0.119	0.083	0.061
<i>d</i> = 3 (E)	<i>i</i> = 1	0.364	0.311	0.287	0.249	0.187	0.132	0.088	0.053	
<i>d</i> = 3 (E)	<i>i</i> = 2	0.365	0.314	0.290	0.251	0.188	0.131	0.088	0.052	
<i>d</i> = 3 (E)	<i>i</i> = 3	0.363	0.308	0.283	0.247	0.185	0.131	0.087	0.053	
<i>d</i> = 4 (SE)	<i>i</i> = 1	0.342	0.280	0.256	0.218	0.174	0.131	0.097	0.069	0.045
<i>d</i> = 4 (SE)	<i>i</i> = 2	0.344	0.279	0.259	0.225	0.176	0.133	0.101	0.074	0.051
<i>d</i> = 4 (SE)	<i>i</i> = 3	0.342	0.275	0.259	0.225	0.175	0.133	0.101	0.074	0.054
<i>d</i> = 5 (S)	<i>i</i> = 1	0.350	0.319	0.300	0.268	0.213	0.167	0.127	0.094	0.072
<i>d</i> = 5 (S)	<i>i</i> = 2	0.352	0.324	0.297	0.269	0.214	0.169	0.130	0.094	0.072
<i>d</i> = 5 (S)	<i>i</i> = 3	0.351	0.322	0.296	0.268	0.214	0.168	0.128	0.095	0.072
<i>d</i> = 6 (SW)	<i>i</i> = 1	0.347	0.301	0.274	0.244	0.197	0.154	0.117	0.089	0.061
<i>d</i> = 6 (SW)	<i>i</i> = 2	0.347	0.304	0.273	0.245	0.198	0.154	0.116	0.086	0.059
<i>d</i> = 6 (SW)	<i>i</i> = 3	0.348	0.303	0.274	0.246	0.199	0.156	0.117	0.087	0.059
<i>d</i> = 7 (W)	<i>i</i> = 1	0.346	0.309	0.295	0.268	0.218	0.168	0.114	0.068	
<i>d</i> = 7 (W)	<i>i</i> = 2	0.348	0.312	0.297	0.269	0.220	0.168	0.116	0.067	
<i>d</i> = 7 (W)	<i>i</i> = 3	0.348	0.314	0.297	0.270	0.220	0.169	0.116	0.067	
<i>d</i> = 8 (NW)	<i>i</i> = 1	0.348	0.307	0.280	0.251	0.204	0.162	0.121	0.088	0.053
<i>d</i> = 8 (NW)	<i>i</i> = 2	0.349	0.306	0.281	0.253	0.206	0.163	0.124	0.090	0.057
<i>d</i> = 8 (NW)	<i>i</i> = 3	0.346	0.308	0.281	0.252	0.205	0.162	0.123	0.090	0.056
<i>d</i> = 1 (N)	<i>i</i> = 4	0.340	0.298	0.280	0.251	0.201	0.157	0.119	0.089	0.059
<i>d</i> = 1 (N)	<i>i</i> = 5	0.337	0.296	0.277	0.248	0.200	0.157	0.118	0.087	0.056
<i>d</i> = 1 (N)	<i>i</i> = 6	0.339	0.295	0.278	0.249	0.200	0.158	0.119	0.089	0.066

Table A7. Maximum deflections measured during the 27 FWD tests performed on the old slab A2-50000 [mm].

Test Direction	Test Number	Geophone								
		<i>g</i> = 1	<i>g</i> = 2	<i>g</i> = 3	<i>g</i> = 4	<i>g</i> = 5	<i>g</i> = 6	<i>g</i> = 7	<i>g</i> = 8	<i>g</i> = 9
<i>d</i> = 1 (N)	<i>i</i> = 1	0.407	0.369	0.346	0.315	0.255	0.202	0.155	0.112	0.081
<i>d</i> = 1 (N)	<i>i</i> = 2	0.402	0.360	0.341	0.310	0.253	0.199	0.151	0.109	0.084
<i>d</i> = 1 (N)	<i>i</i> = 3	0.402	0.358	0.339	0.309	0.252	0.198	0.151	0.109	0.084
<i>d</i> = 2 (NE)	<i>i</i> = 1	0.395	0.356	0.335	0.303	0.251	0.200	0.150	0.111	0.080
<i>d</i> = 2 (NE)	<i>i</i> = 2	0.397	0.354	0.335	0.301	0.250	0.200	0.150	0.112	0.084
<i>d</i> = 2 (NE)	<i>i</i> = 3	0.399	0.356	0.336	0.302	0.251	0.200	0.150	0.110	0.082
<i>d</i> = 3 (E)	<i>i</i> = 1	0.398	0.358	0.339	0.310	0.254	0.205	0.156		
<i>d</i> = 3 (E)	<i>i</i> = 2	0.401	0.357	0.344	0.311	0.258	0.206	0.158		
<i>d</i> = 3 (E)	<i>i</i> = 3	0.400	0.358	0.340	0.311	0.255	0.207	0.158		
<i>d</i> = 4 (SE)	<i>i</i> = 1	0.396	0.345	0.338	0.310	0.250	0.200	0.275	0.112	0.074
<i>d</i> = 4 (SE)	<i>i</i> = 2	0.397	0.347	0.330	0.304	0.246	0.203	0.157	0.113	0.081
<i>d</i> = 4 (SE)	<i>i</i> = 3	0.398	0.351	0.332	0.306	0.263	0.203	0.158	0.114	0.080
<i>d</i> = 5 (S)	<i>i</i> = 1	0.394	0.365	0.348	0.323	0.276	0.221	0.175	0.134	0.096
<i>d</i> = 5 (S)	<i>i</i> = 2	0.394	0.360	0.347	0.323	0.273	0.222	0.172	0.137	0.088
<i>d</i> = 5 (S)	<i>i</i> = 3	0.398	0.368	0.349	0.323	0.275	0.225	0.174	0.138	0.092
<i>d</i> = 6 (SW)	<i>i</i> = 1	0.393	0.344	0.317	0.287	0.236	0.184	0.136	0.098	0.070
<i>d</i> = 6 (SW)	<i>i</i> = 2	0.391	0.344	0.317	0.287	0.236	0.186	0.140	0.101	0.074
<i>d</i> = 6 (SW)	<i>i</i> = 3	0.391	0.344	0.319	0.287	0.236	0.187	0.139	0.100	0.072
<i>d</i> = 7 (W)	<i>i</i> = 1	0.389	0.346	0.325	0.284	0.222	0.169	0.117	0.077	
<i>d</i> = 7 (W)	<i>i</i> = 2	0.393	0.359	0.319	0.286	0.224	0.166	0.117	0.075	
<i>d</i> = 7 (W)	<i>i</i> = 3	0.394	0.348	0.321	0.285	0.223	0.169	0.118	0.075	
<i>d</i> = 8 (NW)	<i>i</i> = 1	0.398	0.345	0.318	0.284	0.225	0.173	0.125	0.091	0.065
<i>d</i> = 8 (NW)	<i>i</i> = 2	0.396	0.344	0.318	0.284	0.225	0.172	0.122	0.088	0.061
<i>d</i> = 8 (NW)	<i>i</i> = 3	0.394	0.344	0.318	0.284	0.225	0.172	0.124	0.088	0.063
<i>d</i> = 1 (N)	<i>i</i> = 4	0.395	0.353	0.333	0.301	0.244	0.193	0.145	0.106	0.075
<i>d</i> = 1 (N)	<i>i</i> = 5	0.397	0.354	0.333	0.302	0.245	0.194	0.146	0.106	0.073
<i>d</i> = 1 (N)	<i>i</i> = 6	0.396	0.354	0.334	0.302	0.245	0.194	0.144	0.106	0.072

Table A8. Maximum deflections measured during the 27 FWD tests performed on the new slab A2-51995 [mm].

Test Direction	Test Number	Geophone								
		$g=1$	$g=2$	$g=3$	$g=4$	$g=5$	$g=6$	$g=7$	$g=8$	$g=9$
$d=1$ (N)	$i=1$	0.370	0.316	0.289	0.256	0.200	0.150	0.109	0.079	0.060
$d=1$ (N)	$i=2$	0.370	0.311	0.283	0.249	0.194	0.143	0.105	0.075	0.062
$d=1$ (N)	$i=3$	0.366	0.312	0.289	0.254	0.196	0.146	0.106	0.075	0.058
$d=2$ (NE)	$i=1$	0.367	0.313	0.291	0.256	0.199	0.151	0.108	0.078	0.055
$d=2$ (NE)	$i=2$	0.368	0.314	0.289	0.256	0.199	0.151	0.107	0.077	0.054
$d=2$ (NE)	$i=3$	0.369	0.315	0.290	0.257	0.200	0.152	0.109	0.076	0.057
$d=3$ (E)	$i=1$	0.368	0.316	0.290	0.254	0.193	0.139	0.094		
$d=3$ (E)	$i=2$	0.371	0.318	0.292	0.257	0.193	0.140	0.095		
$d=3$ (E)	$i=3$	0.372	0.318	0.294	0.257	0.195	0.142	0.093		
$d=4$ (SE)	$i=1$	0.370	0.283	0.262	0.224	0.173	0.128	0.091	0.066	0.046
$d=4$ (SE)	$i=2$	0.371	0.287	0.254	0.226	0.174	0.130	0.092	0.065	0.048
$d=4$ (SE)	$i=3$	0.370	0.286	0.257	0.226	0.173	0.128	0.091	0.066	0.047
$d=5$ (S)	$i=1$	0.367	0.315	0.281	0.252	0.193	0.143	0.103	0.072	0.050
$d=5$ (S)	$i=2$	0.369	0.313	0.283	0.255	0.190	0.144	0.106	0.071	0.048
$d=5$ (S)	$i=3$	0.368	0.313	0.284	0.255	0.191	0.143	0.106	0.071	0.044
$d=6$ (SW)	$i=1$	0.372	0.277	0.247	0.213	0.156	0.113	0.079	0.055	0.043
$d=6$ (SW)	$i=2$	0.372	0.289	0.248	0.213	0.153	0.113	0.079	0.056	0.046
$d=6$ (SW)	$i=3$	0.373	0.287	0.249	0.211	0.146	0.114	0.079	0.055	0.044
$d=7$ (W)	$i=1$	0.370	0.305	0.272	0.233	0.168	0.114			
$d=7$ (W)	$i=2$	0.372	0.306	0.268	0.233	0.168	0.114			
$d=7$ (W)	$i=3$	0.370	0.305	0.267	0.235	0.169	0.114			
$d=8$ (NW)	$i=1$	0.370	0.297	0.267	0.232	0.172	0.123	0.086	0.059	0.041
$d=8$ (NW)	$i=2$	0.371	0.299	0.271	0.233	0.173	0.124	0.086	0.060	0.042
$d=8$ (NW)	$i=3$	0.372	0.300	0.269	0.233	0.174	0.125	0.086	0.059	0.041
$d=1$ (N)	$i=4$	0.370	0.315	0.286	0.252	0.194	0.147	0.104	0.075	0.055
$d=1$ (N)	$i=5$	0.373	0.315	0.287	0.252	0.193	0.145	0.104	0.076	0.055
$d=1$ (N)	$i=6$	0.374	0.319	0.285	0.252	0.193	0.144	0.105	0.077	0.055

Table A9. Maximum deflections measured during the 27 FWD tests performed on the old slab A2-54003 [mm].

Test Direction	Test Number	Geophone								
		$g=1$	$g=2$	$g=3$	$g=4$	$g=5$	$g=6$	$g=7$	$g=8$	$g=9$
$d=1$ (N)	$i=1$	0.671	0.624	0.596	0.552	0.473	0.388	0.303	0.228	0.156
$d=1$ (N)	$i=2$	0.676	0.624	0.603	0.556	0.476	0.389	0.304	0.227	0.157
$d=1$ (N)	$i=3$	0.676	0.621	0.604	0.557	0.474	0.391	0.305	0.229	0.156
$d=2$ (NE)	$i=1$	0.676	0.630	0.607	0.563	0.482	0.396	0.299	0.233	0.166
$d=2$ (NE)	$i=2$	0.677	0.630	0.609	0.565	0.484	0.398	0.300	0.235	0.167
$d=2$ (NE)	$i=3$	0.676	0.634	0.607	0.564	0.481	0.396	0.312	0.234	0.167
$d=3$ (E)	$i=1$	0.670	0.630	0.610	0.564	0.475	0.376	0.273	0.174	
$d=3$ (E)	$i=2$	0.676	0.636	0.613	0.566	0.476	0.377	0.274	0.176	
$d=3$ (E)	$i=3$	0.680	0.638	0.614	0.566	0.476	0.378	0.275	0.176	
$d=4$ (SE)	$i=1$	0.670	0.621	0.595	0.548	0.470	0.392	0.310	0.235	0.169
$d=4$ (SE)	$i=2$	0.676	0.617	0.596	0.550	0.471	0.394	0.309	0.233	0.168
$d=4$ (SE)	$i=3$	0.676	0.620	0.596	0.549	0.472	0.394	0.311	0.234	0.168
$d=5$ (S)	$i=1$	0.672	0.634	0.610	0.569	0.490	0.416	0.333	0.258	0.193
$d=5$ (S)	$i=2$	0.673	0.632	0.616	0.570	0.493	0.418	0.334	0.260	0.191
$d=5$ (S)	$i=3$	0.674	0.632	0.616	0.571	0.493	0.418	0.335	0.261	0.192
$d=6$ (SW)	$i=1$	0.672	0.579	0.539	0.491	0.400	0.312	0.228	0.151	0.096
$d=6$ (SW)	$i=2$	0.675	0.578	0.540	0.491	0.399	0.314	0.229	0.154	0.097
$d=6$ (SW)	$i=3$	0.674	0.577	0.541	0.491	0.401	0.314	0.228	0.155	0.096
$d=7$ (W)	$i=1$	0.663	0.586	0.552	0.487	0.369	0.251	0.133		
$d=7$ (W)	$i=2$	0.668	0.590	0.556	0.491	0.372	0.252	0.136		
$d=7$ (W)	$i=3$	0.669	0.592	0.556	0.492	0.373	0.253	0.138		
$d=8$ (NW)	$i=1$	0.665	0.583	0.551	0.495	0.401	0.310	0.222	0.149	0.094
$d=8$ (NW)	$i=2$	0.668	0.584	0.554	0.497	0.402	0.312	0.222	0.149	0.094
$d=8$ (NW)	$i=3$	0.668	0.585	0.554	0.498	0.403	0.312	0.221	0.149	0.094
$d=1$ (N)	$i=4$	0.660	0.607	0.583	0.538	0.457	0.373	0.297	0.220	0.147
$d=1$ (N)	$i=5$	0.661	0.609	0.587	0.538	0.457	0.372	0.294	0.220	0.150
$d=1$ (N)	$i=6$	0.663	0.609	0.586	0.538	0.458	0.374	0.295	0.219	0.150

Table A10. Maximum deflections measured during the 27 FWD tests performed on the new slab A2-54440 [mm].

Test Direction	Test Number	Geophone								
		$g=1$	$g=2$	$g=3$	$g=4$	$g=5$	$g=6$	$g=7$	$g=8$	$g=9$
$d=1$ (N)	$i=1$	0.336	0.284	0.259	0.229	0.178	0.138	0.105	0.078	0.060
$d=1$ (N)	$i=2$	0.337	0.281	0.257	0.227	0.176	0.136	0.106	0.080	0.057
$d=1$ (N)	$i=3$	0.338	0.282	0.257	0.227	0.174	0.136	0.101	0.077	0.060
$d=2$ (NE)	$i=1$	0.334	0.278	0.257	0.224	0.174	0.133	0.101	0.075	0.061
$d=2$ (NE)	$i=2$	0.336	0.279	0.259	0.225	0.176	0.134	0.102	0.076	0.060
$d=2$ (NE)	$i=3$	0.337	0.280	0.257	0.225	0.175	0.135	0.102	0.076	0.060
$d=3$ (E)	$i=1$	0.339	0.275	0.249	0.219	0.167	0.127	0.091	0.063	
$d=3$ (E)	$i=2$	0.340	0.276	0.251	0.220	0.167	0.127	0.092	0.063	
$d=3$ (E)	$i=3$	0.338	0.276	0.251	0.221	0.167	0.127	0.091	0.063	
$d=4$ (SE)	$i=1$	0.336	0.254	0.235	0.197	0.158	0.125	0.087	0.067	0.050
$d=4$ (SE)	$i=2$	0.338	0.256	0.239	0.201	0.159	0.128	0.085	0.068	0.049
$d=4$ (SE)	$i=3$	0.338	0.254	0.242	0.200	0.160	0.127	0.088	0.068	0.049
$d=5$ (S)	$i=1$	0.329	0.276	0.253	0.220	0.179	0.134	0.099	0.081	0.057
$d=5$ (S)	$i=2$	0.334	0.279	0.250	0.221	0.171	0.135	0.109	0.077	0.058
$d=5$ (S)	$i=3$	0.333	0.280	0.249	0.221	0.172	0.132	0.105	0.079	0.058
$d=6$ (SW)	$i=1$	0.338	0.251	0.226	0.199	0.150	0.117	0.085	0.063	0.046
$d=6$ (SW)	$i=2$	0.338	0.251	0.225	0.199	0.151	0.117	0.084	0.063	0.045
$d=6$ (SW)	$i=3$	0.338	0.252	0.224	0.199	0.149	0.117	0.084	0.063	0.045
$d=7$ (W)	$i=1$	0.331	0.266	0.241	0.211	0.160	0.117	0.077		
$d=7$ (W)	$i=2$	0.333	0.269	0.244	0.213	0.161	0.120	0.079		
$d=7$ (W)	$i=3$	0.331	0.268	0.246	0.212	0.160	0.116	0.075		
$d=8$ (NW)	$i=1$	0.334	0.266	0.243	0.213	0.163	0.124	0.089	0.066	0.049
$d=8$ (NW)	$i=2$	0.335	0.268	0.243	0.214	0.164	0.126	0.090	0.067	0.049
$d=8$ (NW)	$i=3$	0.337	0.269	0.241	0.211	0.165	0.125	0.090	0.064	0.047
$d=1$ (N)	$i=4$	0.334	0.276	0.254	0.221	0.173	0.135	0.102	0.077	0.060
$d=1$ (N)	$i=5$	0.335	0.276	0.257	0.222	0.174	0.139	0.102	0.079	0.059
$d=1$ (N)	$i=6$	0.335	0.277	0.255	0.223	0.174	0.140	0.102	0.079	0.058